

Snail1-dependent p53 repression regulates expansion and activity of tumour-initiating cells in breast cancer

Ting Ni^{1,7}, Xiao-Yan Li^{2,7}, Na Lu^{1,7}, Teng An¹, Zhi-Ping Liu³, Rong Fu¹, Wen-Cong Lv¹, Yi-Wei Zhang¹, Xiao-Jun Xu¹, R. Grant Rowe², Yong-Shun Lin², Amanda Scherer², Tamar Feinberg², Xiao-Qi Zheng⁴, Bao-An Chen⁵, X. Shirley Liu⁶, Qing-Long Guo¹, Zhao-Qiu Wu^{1,8} and Stephen J. Weiss^{2,8}

The zinc-finger transcription factor Snail1 is inappropriately expressed in breast cancer and associated with poor prognosis. While interrogating human databases, we uncovered marked decreases in relapse-free survival of breast cancer patients expressing high *Snail1* levels in tandem with wild-type, but not mutant, p53. Using a Snail1 conditional knockout model of mouse breast cancer that maintains wild-type p53, we find that Snail1 plays an essential role in tumour progression by controlling the expansion and activity of tumour-initiating cells in preneoplastic glands and established tumours, whereas it is not required for normal mammary development. Growth and survival of preneoplastic as well as neoplastic mammary epithelial cells is dependent on the formation of a Snail1/HDAC1/p53 tri-molecular complex that deacetylates active p53, thereby promoting its proteasomal degradation. Our findings identify Snail1 as a molecular bypass that suppresses the anti-proliferative and pro-apoptotic effects exerted by wild-type p53 in breast cancer.

Oncogenic events precipitate the activation of gene programs that trigger either permanent withdrawal from the cell cycle or apoptosis^{1–3}. The p53 tumour suppressor network is a critical regulator of cellular responses to oncogenic stress, and is a frequent mutational target in human cancers³. However, most human breast cancer patients express wild-type p53 and the mechanisms that allow bypass of this critical ‘guardian of the genome’ during oncogenic transformation remain speculative³. Interestingly, recent attention has focused on the function of the zinc-finger (ZF) transcription factor Snail1 in breast cancer^{4–9}. Following its over-expression in transformed mammary epithelial cells (MaECs), Snail1 promotes an epithelial–mesenchymal transition (EMT) program and the acquisition of stem cell-like characteristics while enhancing tumorigenicity^{5–12}. However, Snail1 expression normally falls under the control of complex transcriptional and post-transcriptional regulatory networks¹², and the role of the endogenously derived gene product in tumour progression remains largely unexplored. As early studies described an association between *Snail1* messenger RNA levels and relapse-free survival in breast cancer patients⁴, we re-investigated links between *Snail1* mRNA expression

and survival in human patients expressing wild-type or mutant p53, while launching efforts to define the role of Snail1 in regulating breast cancer progression *in vivo*.

RESULTS

Increased *Snail1* expression worsens relapse-free survival rates in women with breast cancer in a *TP53* wild-type-dependent fashion

In female breast cancer patients, *TP53* mutations are relegated to a subset of approximately 25% of the disease cohort³. While examining relationships between *Snail1* mRNA expression levels and clinical outcomes^{13,14}, we noted an inverse relationship between *Snail1* levels and relapse-free survival (RFS) in patients expressing wild-type, but not mutant, *TP53* (Fig. 1a). More subtle, but nevertheless, significant associations are also established between *Snail1* and distant -metastasis-free survival as well as overall survival in wild-type, but not mutant, *TP53* patients (Fig. 1b,c). Segregating the patient cohort expressing wild-type *TP53* into three major molecular subtypes (that is, luminal, HER2⁺ and basal breast cancer), a significant association

¹State Key Laboratory of Natural Medicines, Jiangsu Provincial Key Laboratory of Carcinogenesis and Intervention, Department of Basic Medicine, School of Basic Medicine and Clinical Pharmacy, China Pharmaceutical University, Nanjing 210009, China. ²Division of Molecular Medicine and Genetics, Department of Internal Medicine, The Life Sciences Institute, University of Michigan, Ann Arbor, Michigan 48109, USA. ³Department of Biochemistry and Molecular Biology, School of Basic Medicine, Gannan Medical University, Ganzhou 341000, China. ⁴Department of Mathematics, Shanghai Normal University, Shanghai 200234, China. ⁵Department of Hematology and Oncology, The Affiliated Zhongda Hospital, Southeast University Medical School, Nanjing 210009, China. ⁶Department of Biostatistics and Computational Biology, The Dana-Farber Cancer Institute, Harvard School of Public Health, Harvard University, Boston, Massachusetts 02115, USA. ⁷These authors contributed equally to this work.

⁸Correspondence should be addressed to Z.-Q.W. or S.J.W. (e-mail: zqw@cpu.edu.cn or sjweiss@umich.edu)

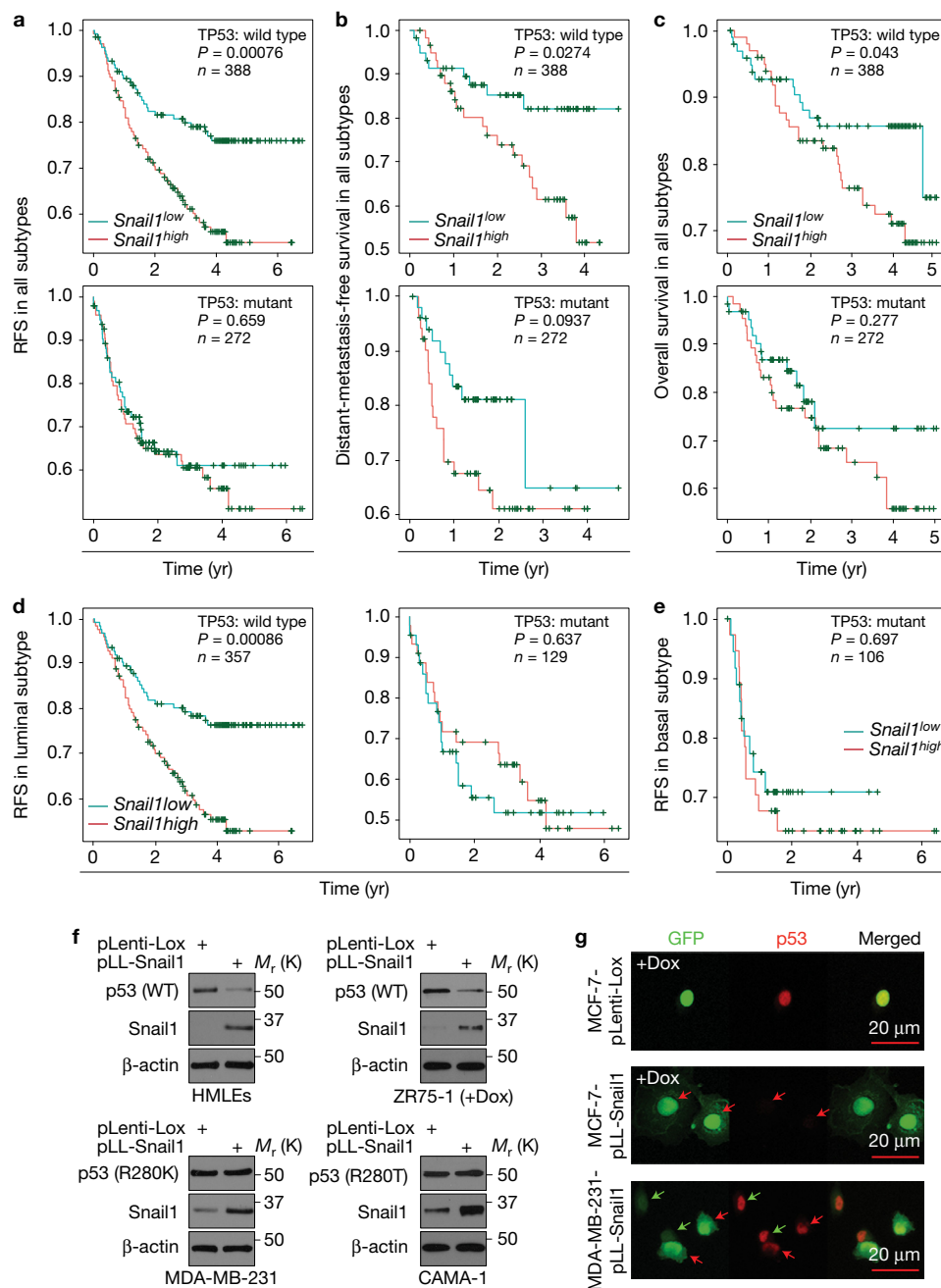


Figure 1 Snail1 expression levels correlate negatively with breast cancer patient survival harbouring wild-type, but not mutant, *TP53* alleles. (**a–c**) Kaplan–Meier survival analysis establishes a relationship between relapse-free survival (RFS; **a**), distant-metastasis-free survival (**b**) and overall survival (**c**) rates and *Snail1* expression level in all subtypes of breast cancer patients bearing wild-type or mutant *TP53* alleles. Survivals are fitted by the ‘survfit’ function. Kaplan–Meier curves are drawn by the ‘ggsurv’ function in the R package ‘survival’. Differences between two survival curves are measured by the G-rho family of tests. n represents the number of patients. (**d,e**) Kaplan–Meier survival analysis of the relationship between RFS rate and *Snail1* expression level in luminal (**d**) or basal (**e**) subtypes of breast cancer patients harbouring wild-type or mutant *TP53* alleles. n represents

the number of patients. G-rho family of tests. (**f**) Following transduction with a *Snail1* expression vector, endogenous wild-type p53 levels were repressed in HMLEs and ZR75-1 cells, but not in MDA-MB-231 or CAMA-1 cells that express mutant p53. Cells were infected with pLenti-Lox-IRES-eGFP (pLenti-Lox) or pLenti-Lox-IRES-eGFP-*Snail1* (pLL-*Snail1*) expression vectors; GFP-positive cells were sorted by FACS and subjected to western blot analysis. (**g**) MCF-7 cells or MDA-MB-231 cells were infected with control or *Snail1* expression vectors as shown in **f**, but without FACS. MCF-7 cells were treated with doxorubicin to induce p53 expression whereas untreated MDA-MB-231 cells were visualized by immunofluorescence. Results are representatives of three independent experiments (**f,g**). Unprocessed original scans of blots are shown in Supplementary Fig. 8.

is identified between *Snail1* and RFS in luminal, but not basal or HER2⁺ subtypes (largely a consequence of the limited number of patients with wild-type *TP53* in these last groups) (Fig. 1d and

Supplementary Fig. 1a,b). This inverse relationship is absent in all three subtypes of patient harbouring mutant *TP53* (Fig. 1d,e and Supplementary Fig. 1a). As the ability of *Snail1* to affect p53 function

remains controversial^{15–19}, we determined the impact of Snail1 on p53 levels in normal or neoplastic human MaECs expressing either wild-type or mutant *TP53*. Following transduction with a Snail1 expression vector, wild-type p53 protein levels fall in normal MaECs or breast cancer cells (Fig. 1f,g). By contrast, exogenously introduced Snail1 did not affect mutant (R280K or R280T) p53 protein levels in human breast carcinoma cells (Fig. 1f,g). Taken together, these results mirror the status of the patient cohort wherein Snail1—directly or indirectly—serves as a suppressor of wild-type, but not mutant, p53.

Conditional deletion of Snail1 in MaECs restrains the formation and metastatic potential of PyMT-induced mammary tumours

To identify potential roles for endogenously derived Snail1 during tumour progression *in vivo*, we generated both Snail1^{LacZ/wt} and Snail1^{fl/fl} mice^{20–23}, and crossed these transgenic lines into the MMTV-PyMT mouse model of breast cancer^{24,25}. MMTV-PyMT transgenic mice exhibit multiple similarities to the luminal B subtype of human breast cancer, and progress from benign hyperplasia to an invasive, poorly differentiated carcinoma that displays a metastatic phenotype^{8,9,24–26}. In PyMT-Snail1^{LacZ/wt} mice, reporter activity is widely detected in hyperplastic lesions and established tumours, but not adjacent normal tissues (Fig. 2a,b), a finding consistent with Snail1 expression in human breast cancer^{27–29}.

Using MMTV-Cre transgenic mice (line F) to target Cre expression in MaECs^{30–32}, we crossed MMTV-Cre;Snail1^{fl/fl} conditional knockout (cKO) mice with MMTV-PyMT mice to generate female cohorts with the genotypes of MMTV-PyMT;Snail1^{fl/fl} (designated PyMT-WT mice), MMTV-PyMT;MMTV-Cre;Snail1^{fl/wt} (PyMT-Het mice), and MMTV-PyMT;MMTV-Cre;Snail1^{fl/fl} (PyMT-cKO mice). In PyMT-cKO;ROSA-LacZ reporter mice, β -galactosidase/LacZ activity is detected in the epithelial compartment of both preneoplastic glands and established tumours, complemented by the absence of Snail1 protein in preneoplastic as well as neoplastic MaECs (Fig. 2c,d and Supplementary Fig. 2a,b). In PyMT-WT mice, palpable tumours develop in 45-day-old animals with 50% of the mice displaying frank tumour growth by day 60 (Fig. 2e). In marked contrast, tumour initiation in PyMT-cKO mice is delayed significantly with 50% of targeted mice developing tumours only after 80 days (Fig. 2e). Relative to PyMT-WT controls, whole-mounts of -cKO mammary glands at 15 weeks of age display significant reductions in tumour size (Supplementary Fig. 2c). By 17 weeks of age, while PyMT-WT mice develop multiple tumours, marked reductions in tumour size and number are found in -cKO mice (Fig. 2f,g). Approximately 9 weeks after the initial detection of mammary tumours, PyMT-WT mice develop large numbers of metastatic lung nodules (Fig. 2h). By contrast, 9 weeks after palpable tumours develop in PyMT-cKO mice, Snail1 mRNA levels are decreased by ~80% and few metastatic nodules are detected (see below and Fig. 2h). Circulating tumour cells also demonstrate a marked decrease in *PyMT* mRNA levels in blood recovered from PyMT-cKO mice relative to controls (Fig. 2i). Of note, *PyMT* mRNA levels in primary tumours from PyMT-WT and -cKO groups are comparable, demonstrating that Snail1 does not affect *PyMT* expression (Fig. 2i). Importantly, deleting Snail1 in the normal mammary gland does not affect branching morphogenesis, during either development or pregnancy (Supplementary Fig. 2d).

Loss of Snail1 in MaECs inhibits expansion and activity of PyMT-induced TICs

Mammary gland whole-mounts prepared from PyMT-WT and -cKO mice were next isolated at hyperplastic/preneoplastic stages of growth (6–8 weeks of age) to determine the impact of Snail1 expression on tumour initiation. MMTV-PyMT induces extensive hyperplasia as early as 6 weeks in WT mice^{24,25}, whereas glands from cKO mice exhibit markedly fewer and smaller hyperplastic lesions (Fig. 3a,b). By 8 weeks of age, increased numbers of hyperplastic foci are observed in the more distal regions of the mammary gland in PyMT-WT mice relative to -cKO tissues (Fig. 3a,b).

To define the role of Snail1 in controlling the expansion of transformed MaECs, Lin⁻ epithelial cells were recovered from normal or PyMT preneoplastic mammary glands and profiled using surface markers that distinguish luminal from basal mammary epithelial subsets^{33–35}. The percentage of CD29^{lo}CD24⁺ or CD29^{lo}CD61⁺ subpopulations, representing luminal progenitor cells, in normal glands is comparable between WT and cKO mice (Fig. 3c–e). However, whereas PyMT expands the CD29^{lo}CD24⁺ and CD29^{lo}CD61⁺ subsets in -WT glands, -cKO glands fail to increase luminal progenitors (Fig. 3c–e). By contrast, the percentage of the CD29⁺CD24⁺ basal population, which enriches for mammary stem cells in certain tumour models³⁵, is markedly decreased in PyMT-WT mammary glands relative to -cKO glands (Supplementary Fig. 3a). While CD29^{lo}CD24⁺/CD24⁺CD90⁺, but not CD29⁺CD24⁺, subsets have been reported to exhibit tumour-initiating cell (TIC) properties in PyMT-induced tumours^{36,37}, the percentage of CD24⁺CD90⁺ cells is comparable between PyMT-WT and -cKO preneoplastic glands (Supplementary Fig. 3b,c).

To assess the effect of Snail1 ablation on TIC status, we isolated preneoplastic mammary epithelial cells (pNECs) from PyMT-WT and -cKO mice, and performed *in vitro* mammosphere assays. pNECs from PyMT-cKO mice display a marked reduction in mammosphere number and size relative to -WT controls (Fig. 3f and Supplementary Fig. 3d). Furthermore, corroborating our *in vitro* findings, when limiting numbers of pNECs are injected orthotopically, the PyMT-cKO-derived pNECs display reduced TIC potential (Fig. 3g,h). Similar requirements for Snail1 are observed when preneoplastic mammary luminal progenitor cells (CD29^{lo}CD24⁺) are recovered from MMTV-PyMT;Snail1^{fl/fl} mice, transduced with adeno- β Gal or -Cre in short-term culture and transplanted orthotopically (Fig. 3i–k).

PyMT-cKO tumours retain a differentiated status and exhibit an impaired collective cell invasion phenotype

At 9 weeks, PyMT-WT glands progress to early carcinomas with a loss of normal epithelial architecture (Fig. 4a)⁹. By contrast, glands from PyMT-cKO mice maintain features of well-differentiated adenomas that retain portions of normal ductal structures (Fig. 4a). At 13 weeks and beyond, PyMT-WT glands progress to poorly differentiated adenocarcinomas, whereas glands from -cKO mice exhibit a marked delay in tumour progression and a more differentiated phenotype (Fig. 4a, middle and right panels). Indeed, β -casein, a well-characterized luminal differentiation marker^{34,35}, is increased in tandem with other differentiation markers in PyMT-cKO tissues (Fig. 4b,c). Hence, Snail1 either actively promotes the acquisition of a de-differentiated phenotype or alternatively, interferes with normal stem cell differentiation³⁴.

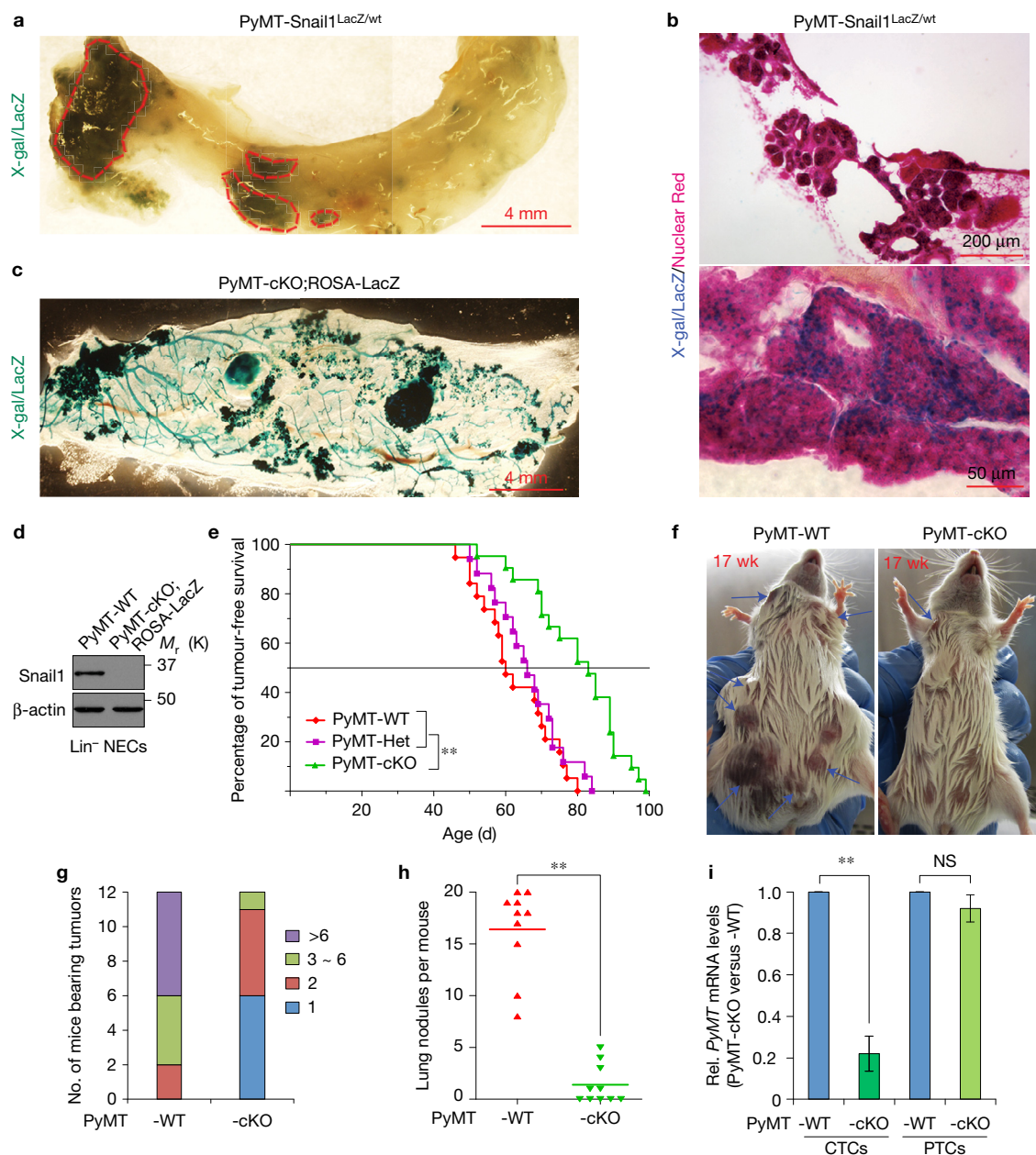


Figure 2 Conditional deletion of *Snail1* in MaECs restrains the formation and metastatic potential of MMTV-PyMT-induced mammary tumours. **(a)** Whole-mount X-gal/LacZ staining of mammary glands from 10-week-old PyMT-Snail1^{LacZ/wt} mice (the image is representative of images from five mice). Areas demarcated by dashed lines denote *Snail1*-positive hyperplastic and neoplastic lesions. **(b)** Cross-sections of mammary glands as shown in **a** were stained with X-gal/LacZ (the image is representative of images from five mice). **(c)** Whole-mount X-gal/LacZ staining of mammary glands from 12-week-old PyMT-cKO;Rosa-LacZ reporter mice (the image is representative of images from five mice). MMTV-Cre is specifically expressed in mammary epithelial cell lineage within affected ductal trees and lesion areas. **(d)** Western blot analysis of Lin⁻NECs derived from mammary glands of 12-week-old PyMT-WT and PyMT-cKO;Rosa-LacZ mice. Results are representatives of five independent experiments. **(e)** Kaplan–Meier analysis of mammary tumour

development in PyMT-WT ($n = 19$ mice), PyMT-Het ($n = 17$ mice), and PyMT-cKO ($n = 19$ mice) female mice. $**P < 0.01$, log-rank test. **(f)** Gross examination of palpable tumours in PyMT-WT (left) and -cKO (right) mice at 17 weeks of age (12 mice, each). Arrows mark tumours that have developed in mice. **(g)** Number of PyMT-WT or -cKO mice as shown in **f** bearing the indicated number of tumours at 17 weeks of age ($n = 12$ mice, each). **(h)** Lungs were harvested from PyMT-WT and -cKO mice ($n = 10$ mice, each) at 10 weeks post-detection of palpable tumours, and metastatic nodules were counted. $**P < 0.01$, Mann–Whitney test. **(i)** The lysates of circulating tumour cells (CTCs) and primary tumour cells (PTCs) were prepared from PyMT-WT and -cKO mice and subjected to RT-qPCR analysis. Data are presented as mean \pm s.e.m. ($n = 5$ independent experiments). $**P < 0.01$, two-sided Student's *t*-test. NS, not significant. Unprocessed original scans of blots are shown in Supplementary Fig. 8.

Snail1 was among the first transcription factors identified to induce EMT^{11,38}, but recent studies have identified key roles for the transcription factor that do not necessarily effect changes in

epithelial–mesenchymal characteristics^{2,21,22,39}. Indeed, isolated neoplastic mammary epithelial cells (NECs) from PyMT-cKO mice display only subtle increases in E-cadherin levels in concert with

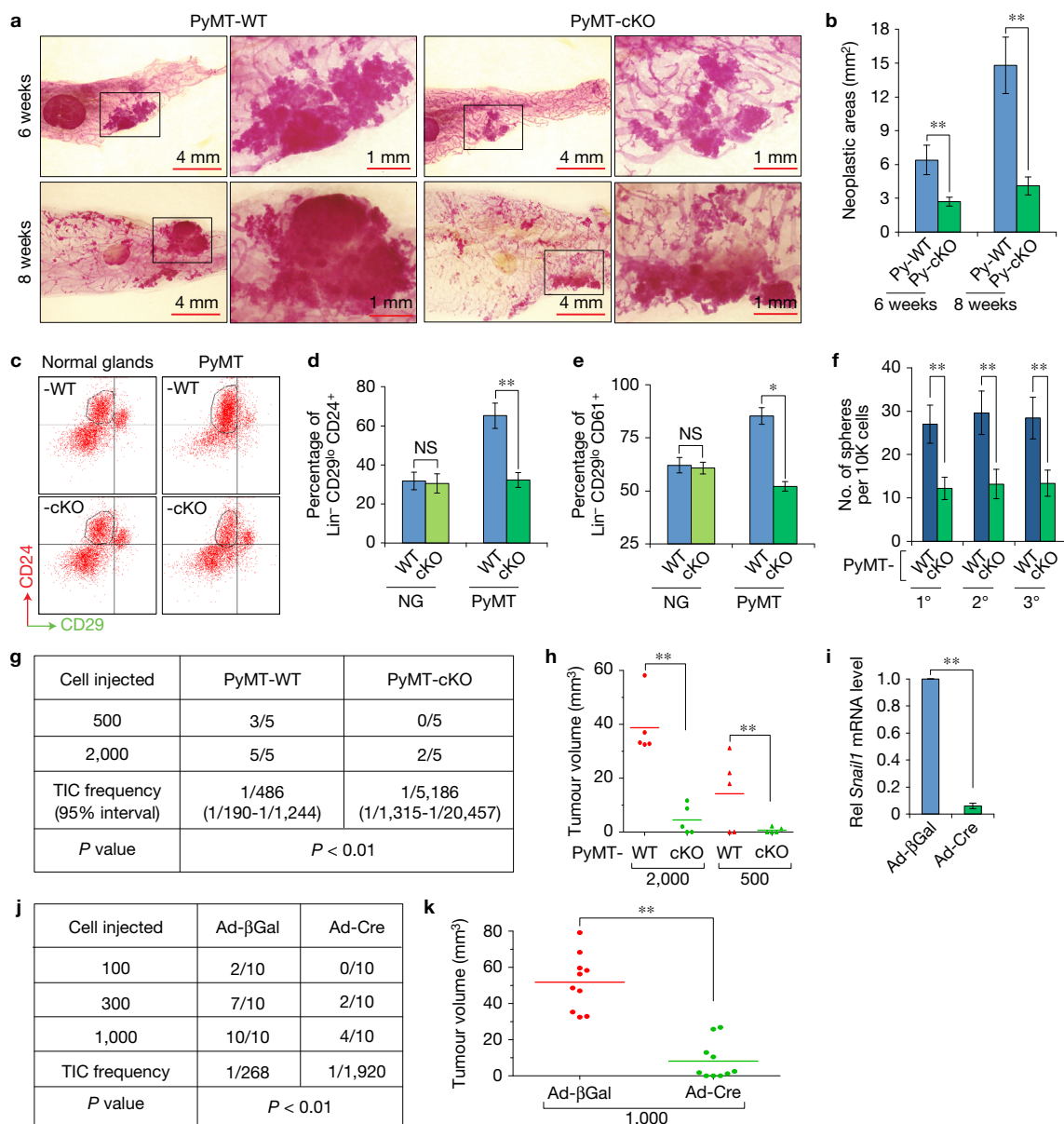


Figure 3 Loss of Snail1 in MaECs inhibits expansion and activity of PyMT-induced TICs. **(a)** Whole-mount carmine red staining of mammary glands from PyMT-WT and -cKO mice at 6 and 8 weeks of age (the image is representative of images from five mice). Magnified areas of boxed sections are shown in the right panels. **(b)** Quantification of neoplastic/hyperplastic areas in the mammary glands as shown in **a**. Data are presented as mean \pm s.e.m. ($n=5$ independent experiments). $**P < 0.01$, two-sided Student's *t*-test. **(c)** Flow cytometry of LIN⁻ MaECs harvested from normal or PyMT preneoplastic mammary glands at 6 weeks of age. The results shown are representative of data obtained from analyses of 6 mice. **(d,e)** Quantification of LIN⁻CD29⁺CD24⁺ **(d)** and LIN⁻CD29⁺CD61⁺ **(e)** TICs analysed at 6 weeks of age. Data are presented as mean \pm s.e.m. ($n=6$ independent experiments). $*P < 0.05$, $**P < 0.01$, two-sided Student's *t*-test. **(f)** Number of tumourspheres formed by PyMT-WT or -cKO pNECs dissected from mammary glands of 6-week-old mice. 1°, 2° and 3° denote the three successive generations of preneoplastic epithelial cells used in the assay, respectively.

Data are presented as mean \pm s.e.m. ($n=6$ independent experiments). $**P < 0.01$, two-sided Student's *t*-test. **(g,h)** pNECs isolated from mammary glands of 6-week-old PyMT-WT or -cKO mice were orthotopically transplanted into nude mouse recipients ($n=5$ mice, each), and tumour incidence **(g)** and volume **(h)** monitored 9 weeks after transplantation. $**P < 0.01$, Mann-Whitney test. **(i)** Preneoplastic mammary luminal progenitor cells (CD29⁺CD24⁺) isolated from 6-week-old PyMT-WT (that is, PyMT-Snail1^{fl/fl}) mice were transduced with adeno-βGal or -Cre in suspension for 2 h. A portion of the transduced cells were cultured *in vitro* for 48 h, and the cell lysates were collected for RT-PCR to assess the efficiency of Snail1 knockdown. Data are presented as mean \pm s.e.m. ($n=5$ independent experiments). $**P < 0.01$, two-sided Student's *t*-test. **(j,k)** A portion of the transduced cells as described in **i** were immediately transplanted orthotopically into nude mouse recipients ($n=10$ mice, each), and tumour incidence **(j)** and volume **(k)** were monitored 9 weeks after transplantation. $**P < 0.01$, Mann-Whitney test. Source data are provided in Supplementary Table 1 **(g,h,j,k)**.

modest changes in the expression levels of the mesenchymal markers (Fig. 4c). Cytokeratin-14 (K14)-positive, invasive leader cancer cells have been identified at the tumour-stromal cell interface in

both mouse breast cancer models and human patients²⁶, and we likewise find that K14⁺ cells are enriched at the protrusive border of PyMT-WT adenocarcinomas, forming multi-cellular strands that

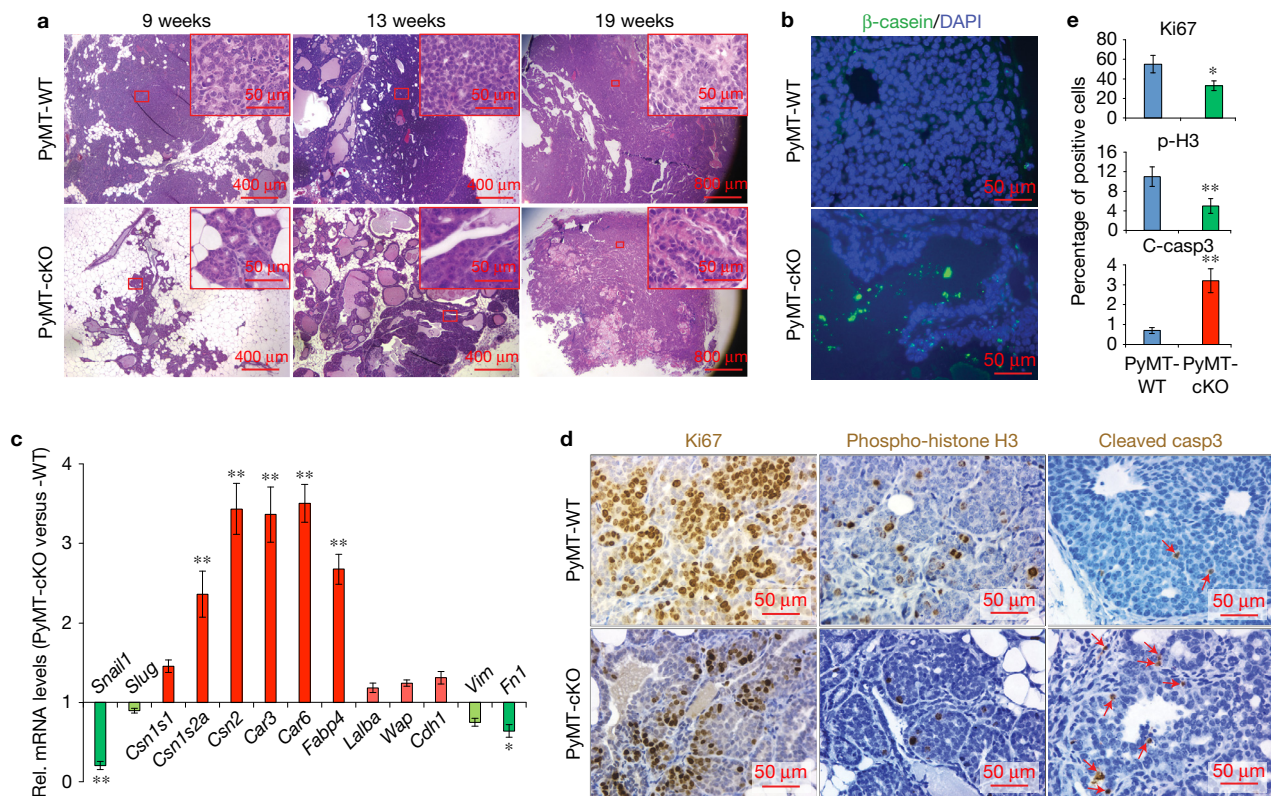


Figure 4 PyMT-cKO tumours retain differentiated status and exhibit impaired growth responses. **(a)** H&E staining of primary tumours from 9-week-, 13-week- or 19-week-old PyMT-WT or -cKO mice (images are representative of images from five mice). Insets display higher magnifications of boxed areas. **(b)** β -Casein immunofluorescent staining of primary tumours from 13-week-old PyMT-WT or PyMT-cKO mice (images are representative of images from five mice). Nuclei are counterstained with DAPI. **(c)** NECs isolated from primary tumours of 19-week-old PyMT-WT or -cKO mice and subjected to qRT-PCR analysis. NECs from PyMT-cKO primary tumours expressed significantly higher levels of multiple differentiation markers with no significant changes in *CDH1* or *Vim* expression. Data are presented

as mean \pm s.e.m. ($n=5$ independent experiments). * $P < 0.05$, ** $P < 0.01$, one-way ANOVA test. **(d)** Immunohistochemical analyses of Ki67, phospho-histone H3 and cleaved caspase 3 in primary tumours derived from 13-week-old PyMT-WT and -cKO mice (images are representative of images from five mice). The arrows in the right panels denote cells positive for cleaved caspase 3 (that is, apoptotic cells). **(e)** Quantification of Ki67-, phospho-histone H3 (p-H3)- and cleaved caspase 3 (C-casp3)-positive cells (%) as shown in **d**. 1,000 to 2,000 cells were counted in 10 random fields of each slide. Data are presented as mean \pm s.e.m. ($n=5$ independent experiments). * $P < 0.05$, ** $P < 0.01$, two-sided Student's *t*-test.

invade into the adjacent stromal tissues (Supplementary Fig. 4a). By contrast, PyMT-cKO adenocarcinomas fail to display a locally invasive phenotype and the K14⁺ tumour cells found within tumour masses retain smooth borders with the surrounding stromal interface (Supplementary Fig. 4a), a finding consistent with the ability of Snail1 to promote tissue-invasive activity^{20,40}.

In addition to triggering EMT, forced expression of Snail1 has been reported to inhibit cell cycle regulation while conferring resistance to pro-apoptotic signals *in vitro*^{11,38}. Nevertheless, in PyMT-cKO mammary glands, we instead find decreased numbers of proliferative and mitotic cells in 4-week-old preneoplastic as well as neoplastic tissues relative to -WT counterparts (Fig. 4d,e and Supplementary Fig. 4b–e). PyMT-cKO mammary glands do, however, display increases in pro-apoptotic cells in both hyperplastic and carcinomatous lesions (Fig. 4d,e and Supplementary Fig. 4b–e).

Snail1 is required to maintain TIC function in established carcinomas

To define the role of Snail1 in maintaining the TIC properties of established carcinomas, LIN⁻ NECs were isolated from late-stage

PyMT-WT carcinomas and transduced with either adeno- β Gal or -Cre before orthotopic injection. Under these conditions, tumours are detected at lower frequency in mice that receive 10² or 10³, but not 10⁴, Snail1-deleted NECs relative to controls (Fig. 5a). Further, tumours generated from 10³, and even 10⁴, Snail1-deleted NECs are dramatically reduced in size relative to controls (Fig. 5b). As these results suggest that Snail1 is required for maintaining TIC function, we profiled LIN⁻ NECs recovered from control and Snail1-deleted orthotopic tumours for CD24, CD29, CD61 and CD90 expression. Unlike the strikingly distinct CD24/CD29/CD61 profiles observed between PyMT-WT and -cKO preneoplastic glands (Fig. 3c–e), comparable CD24/CD29/CD61/CD90 profiles are observed when Snail1 is deleted in advanced NECs (Supplementary Fig. 5a–d). Although these differentiation markers are unable to distinguish between NECs recovered from Snail1-intact versus -deleted tumours, aldehyde dehydrogenase (ALDH) activity can serve as a TIC marker in PyMT-induced breast tumours³⁶. Indeed, ALDH⁺ cells recovered from orthotopic tumours generated by control NECs exhibit higher tumoursphere-forming activity *in vitro* relative to ALDH⁻ cells (Supplementary Fig. 5e–g). Further, the

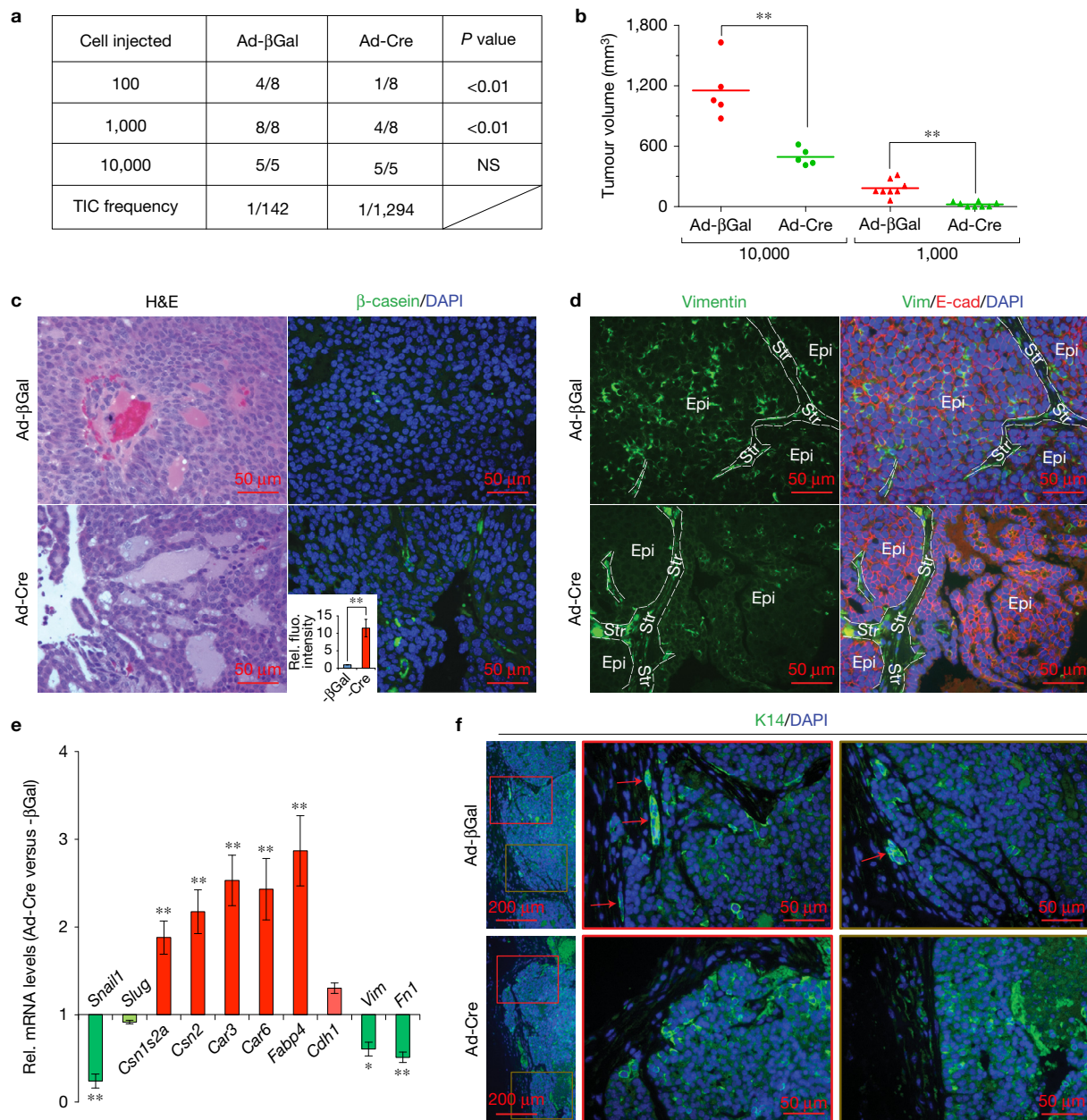


Figure 5 Snail1 maintains carcinoma cell de-differentiation. **(a,b)** NECs were isolated from established tumours of 19-week-old PyMT-WT mice, transduced with adeno- β Gal or -Cre in suspension and orthotopically transplanted into nude mouse recipients ($n=5$ or 8 mice, each). Tumour incidence **(a)** and volume **(b)** were monitored 7 weeks after transplantation. $**P<0.01$, Mann-Whitney test. **(c)** H&E staining (left) and β -casein immunofluorescent staining (right) of transplanted adenocarcinoma cells derived from adeno- β Gal and -Cre transduced neoplastic epithelial cells. Transduced adenocarcinomas were orthotopically injected into nude mice and tumours retrieved 9 weeks post-transplantation (images are representative of images from five orthotopic tumours). Nuclei are DAPI-stained. Relative fluorescent densities of β -casein in 10 random fields of each slide are quantified (insets). Data are presented as mean \pm s.e.m. ($n=5$ independent experiments). $**P<0.01$, two-sided Student's *t*-test.

(d) Vimentin and E-cadherin expression as assessed by immunofluorescent staining of transplanted adenocarcinoma cells as described in **c** (images are representative of images from five mice). Epi, epithelium; Str, stroma. **(e)** NECs were dissociated from transplantable tumours as described in **c**, and subjected to RT-qPCR analysis. Transplanted tumours derived from Snail1-deleted NECs expressed significantly higher levels of differentiation markers. Data are presented as mean \pm s.e.m. ($n=5$ independent experiments). $*P<0.05$, $**P<0.01$, one-way ANOVA test. **(f)** K14 immunofluorescence at the tumour-stromal cell borders of transplanted tumours as shown in **c** (images are representative of images from five mice). Magnified areas of boxed sections (coloured red or brown) are shown to the left in the middle and right panels, respectively. The arrows mark strands of cancer cells that are characteristic of K14⁺ invading leader cells at the tumour-stromal cell interface. Source data are provided in Supplementary Table 1 **(a,b)**.

ALDH⁺ cells copurify with CD29^{lo}CD24⁺/CD29^{lo}CD61⁺ subsets, suggesting that the CD29^{lo}CD24⁺ALDH⁺/CD29^{lo}CD61⁺ALDH⁺ subset functions as TICs in advanced PyMT-induced breast tumours

(Supplementary Fig. 5h,i). Consistent with this premise, the loss in TIC activity observed following Snail1 deletion in transplantation assays (Fig. 5a,b) correlates with a reduction in the ALDH⁺

population (Supplementary Fig. 5i). Likewise, when *Snail1* is deleted in ALDH⁺ cells recovered from PyMT-*Snail1*^{f/f} tumours, tumoursphere-forming activity is reduced (Supplementary Fig. 5j).

To characterize a potential role for *Snail1* in maintaining the de-differentiated phenotype of advanced tumours, MMTV-PyMT;*Snail1*^{f/f} NECs were again isolated from 19-week-old mice, transduced with adeno-βGal or adeno-Cre expression vectors *in vitro* and implanted orthotopically. After 9 weeks, control NECs form poorly differentiated adenocarcinomas (Fig. 5c upper panels). By contrast, orthotopic tumours derived from *Snail1*-deleted NECs recover the ability to partially regenerate ductal architecture and re-express β-casein (Fig. 5c lower panels). Consistent with only minor changes in E-cadherin expression in primary tumours (Fig. 4c), E-cadherin expression is largely maintained in control orthotopic tumours, although staining intensity is increased in *Snail1*-deleted transplanted tumours (Fig. 5d). By contrast, vimentin expression is upregulated in the epithelial compartment of WT control-transplanted orthotopic tumours, but largely restricted to the stroma of *Snail1*-deleted transplants (Fig. 5d). Relative to WT controls, freshly isolated tumours retrieved from transplanted *Snail1*-deleted NECs display significant increases in luminal differentiation markers along with decreased expression of *Vim* and *Fn1* (Fig. 5e). Consistent with their recovered differentiation status, *Snail1*-deleted, K14⁺ carcinoma cells also lose their tissue-invasive potential in tandem with decreased proliferative potential and increased apoptosis (Fig. 5f and Supplementary Fig. 6a,b).

Snail1 acts as a p53 repressor

Given the association between *Snail1* mRNA levels and disease outcome in wild-type *TP53* breast cancer patients, p53 protein levels were assessed immunohistochemically in PyMT-WT versus -cKO preneoplastic glands. Remarkably, p53 levels are increased dramatically in *Snail1*-cKO preneoplastic glands with no detected changes in phospho-Rb levels^{2,41} (Fig. 6a and Supplementary Fig. 6c,f). Similar results are obtained when *Snail1* is excised *in vitro*, the cells injected orthotopically and the transplanted tumours immunostained for p53 and phospho-Rb (Fig. 6b and Supplementary Fig. 6c,f). Although *Snail1* can play a role in controlling genomic integrity^{42,43}, *Snail1*-cKO preneoplastic glands as well as *Snail1*-deleted orthotopic/primary tumours express comparable levels of p-ATM or γ-H2AX relative to controls (Supplementary Fig. 6d-g).

In vitro, while neither adeno-βGal nor adeno-Cre activates p53 expression in PyMT-*Snail1*^{wt/wt} or control floxed tumour cells, *Snail1*-deleted pNECs and NECs increase p53 protein levels, recapitulating the *in vivo* phenotype (Fig. 6c). Further, the downstream p53 targets *p21* and *MDM2*³ are also upregulated with no change in the Rb-associated cyclin kinase inhibitor p16 (Fig. 6c). Although *Snail1* did not affect *TP53* expression, both *p21* and *MDM2* mRNA levels increase significantly in *Snail1*-deleted cells (Supplementary Fig. 7a). Concurrently, *Snail1* decreases p53 half-life while increasing p53 ubiquitylation (Supplementary Fig. 7b,c). Of note, increases in p53 protein levels and activity are also associated with increased levels of p53 acetylation⁴⁴, and following *Snail1* deletion, p53 acetylation (Lys379) levels increase (Fig. 6c). While *Snail1*-dependent decreases in Lys379 acetylation are consistent with a loss in p53 activity, the protein is acetylated at multiple sites that can each play important roles in regulating p53 function⁴⁴. As such, lysates prepared from

Snail1-wild-type or -deleted NECs (containing equalized levels of p53) were subjected to immunoprecipitation using antibodies directed against pan-acetylated lysine (Pan-Ack) or p53. As shown, *Snail1*-deleted NECs display an increased percentage of acetylated p53 molecules (Fig. 6d). Immunofluorescence analysis further illustrates an increase in the levels of co-localized p53 and Pan-Ack in *Snail1*-deleted NECs (Supplementary Fig. 7d). Importantly, the ability of *Snail1* to regulate acetylation-linked events is not limited to p53 as the autocatalytic acetylation of p300, a transcriptional coactivator that acetylates p53^{45,46}, is likewise upregulated in *Snail1*-deleted pNECs and NECs (Fig. 6c).

Consistent with an effect of *Snail1* on p53 acetylation, p53/*Snail1* complexes are found in wild-type NECs with direct binding interactions confirmed using recombinant *Snail1* and p53 (Fig. 6e and Supplementary Fig. 7e)¹⁷. By contrast, a common p53 mutation, that is, Arg280 → Lys280, markedly decreases its binding interaction with *Snail1* in MDA-MB-231 cells (Supplementary Fig. 7f). *Snail1* is divided into a series of domains that encompass the bulk of its transcriptional repressor activity (that is, the SNAG domain) along with four C₂H₂ ZFs that recognize consensus E2-box type elements⁴⁷ (Fig. 6f). Using cells co-expressing epitope-tagged *Snail1* or *Snail1*-deletion mutants and wild-type p53, we identify ZF1 and ZF2 as the dominant p53-binding motifs (Fig. 6f,g). In complementary studies using p53 deletion mutants, wild-type *Snail1* interacts primarily with the DNA-binding domain (DBD) of p53, although ΔN299 p53 mutant retains a weaker, residual binding activity (Fig. 6h,i and Supplementary Fig. 7g). As expected, wild-type, but not ZF1/2-deleted, *Snail1* more effectively represses p53 protein levels in co-expressing cells (Fig. 6j). Interestingly, SNAG domain-deleted *Snail1*, despite maintaining its ability to bind p53, fails to retain its full p53-suppressing activity (Fig. 6j). In considering potential roles for the *Snail1* SNAG domain in p53 repression, earlier studies described the ability of this 9-amino-acid motif to recruit the deacetylase HDAC1⁴⁸. Indeed, while wild-type *Snail1* binds HDAC1 and p53, the SNAG-deleted mutant completely loses its ability to recruit HDAC1 (Fig. 6k). Importantly, when cells are co-transfected with both SNAG domain-deleted *Snail1* and wild-type *Snail1*, the p53 repressive effect of wild-type *Snail1* is abolished (Fig. 6l). With regard to the ZF-deletion mutants of *Snail1*, HDAC1 binding was retained, albeit at lower levels, most likely as a consequence of a decrease in the nuclear import of the *Snail1* mutant⁴⁹. The ability of *Snail1* to act as a bridging molecule between endogenous p53 and HDAC1 is confirmed in co-immunoprecipitation assays wherein *Snail1* deletion almost completely abolishes the recruitment of HDAC1 to p53 (Fig. 6m,n). Consistent with this model, the HDAC inhibitor TSA⁴⁸ blocks the ability of *Snail1* to repress p53 levels while inhibiting p53 deacetylation (Supplementary Fig. 7h).

A Snail1/p53 axis regulates tumorigenic activity

To determine the degree to which p53 serves as a *Snail1* target substrate required for mammary tumour progression, we isolated pNECs from PyMT-cKO glands and assessed the impact of p53 silencing on *in vitro* tumoursphere as well as *in vivo* tumorigenic activity. Immunoblot analysis confirms increased levels of p53 in PyMT-cKO cells with p53 expression largely abolished following *Snail1*/p53 knockdown (Fig. 7a). Importantly, while *Snail1* deletion

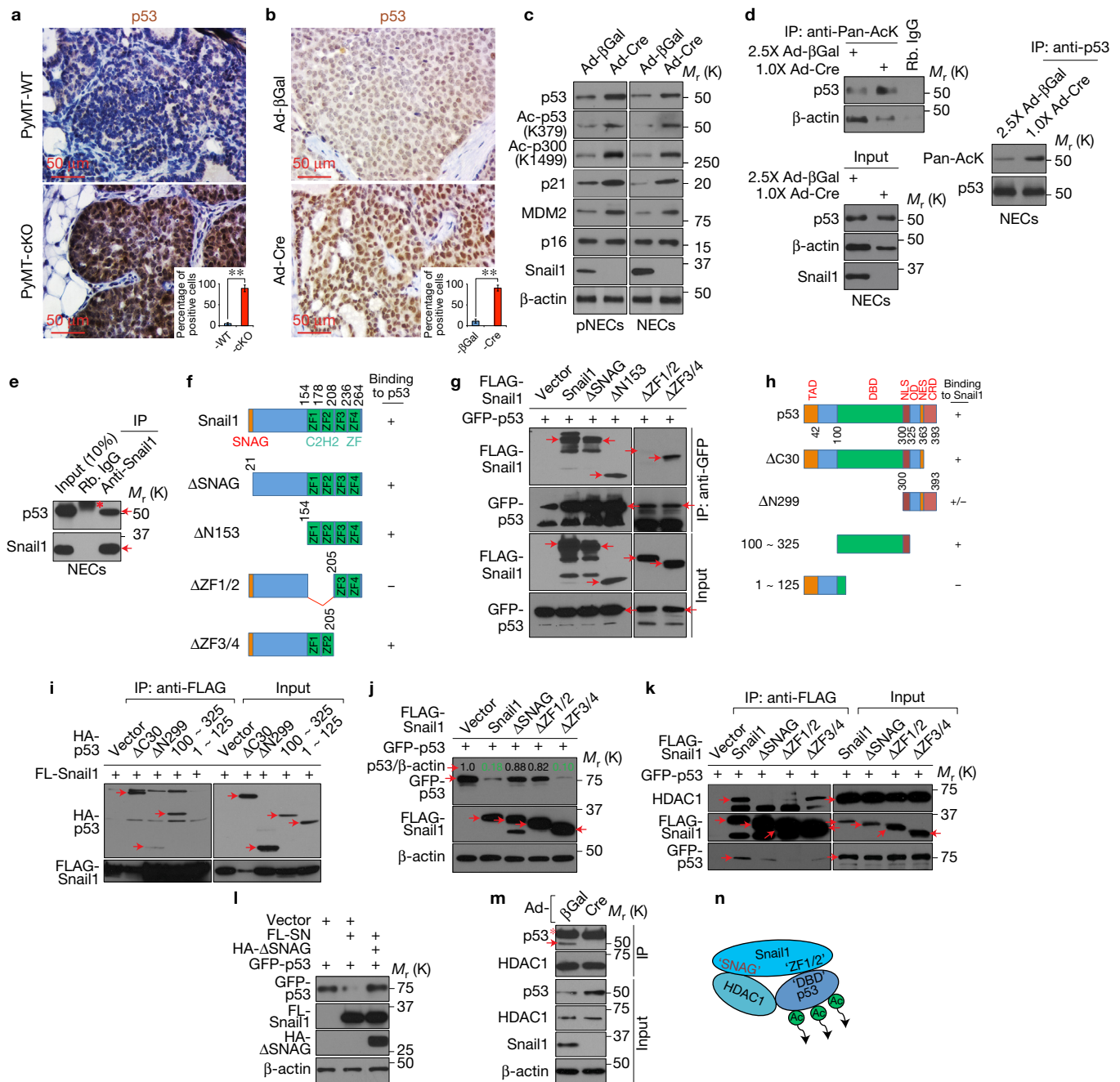


Figure 6 Snail1 acts as a p53 repressor. (a,b) Immunohistochemical staining of p53 in preneoplastic glands of PyMT-WT or -cKO mice (a; images are representative of images from five mice) or formed from wild-type NECs that were transduced with adeno-βGal or -Cre prior to transplantation (b; images are representative of images from five mice). Insets, 1,000 to 2,000 cells were counted in 10 random fields of each slide. Data are presented as mean ± s.e.m. ($n=5$ independent experiments). ** $P < 0.01$, two-sided Student's t -test. (c) pNECs or NECs were recovered from 7-week-old or 19-week-old PyMT-WT mice, respectively. Cells were transduced with adeno-βGal or -Cre, and cell lysates used for immunoblotting. (d) Lysates from adeno-βGal or -Cre transduced NECs loaded at a ratio of 2.5:1 were subjected to immunoprecipitation (IP) assay. (e) Lysates from wild-type NECs were subjected to co-IP assay. (f) Schematic representation of Snail1 protein mutants. (g) 293T cells were co-transfected with equal amounts of Snail1 or Snail1 mutant plasmids and treated with MG132 (10 μM) for 6 h. Cell lysates were prepared and subjected to co-IP assay. (h) Schematic representation of p53 protein mutants. (i) 293T cells were co-transfected with equal amounts

of p53 mutant plasmids and treated with MG132 (10 μM) for 6 h. Cell lysates were prepared and subjected to co-IP assay. Note the weak band from ΔN299 transfectant. (j) 293T cells were co-transfected with GFP-p53 and FLAG-Snail1 (or -deleted mutants) at a ratio of 1:10, and cell lysates were used for immunoblotting. (k) 293T cells were co-transfected with equal amounts of GFP-p53 and FLAG-tagged Snail1 (or -deleted mutants). Cell lysates were prepared and subjected to co-IP assay. (l) 293T cells were co-transfected with GFP-p53, FLAG-Snail1 and HA-Snail1-ΔSNAG at a ratio of 1:10:10, and cell lysates were used for immunoblotting. (m) Lysates from NECs as described in c were subjected to co-IP assay using anti-HDAC1 antibody. (n) A schematic representation of the Snail1/p53/HDAC1 tri-molecular complex with the binding domains responsible for interactions of Snail1-p53 and Snail1-HDAC1. Asterisks and arrows denote IgGs and specific bands with their expected molecular weights, respectively. Results are representative of three (g,i-l) or five (c,d,e,m) independent experiments. Unprocessed original scans of blots are shown in Supplementary Fig. 8. Source data are provided in Supplementary Table 1 (j).

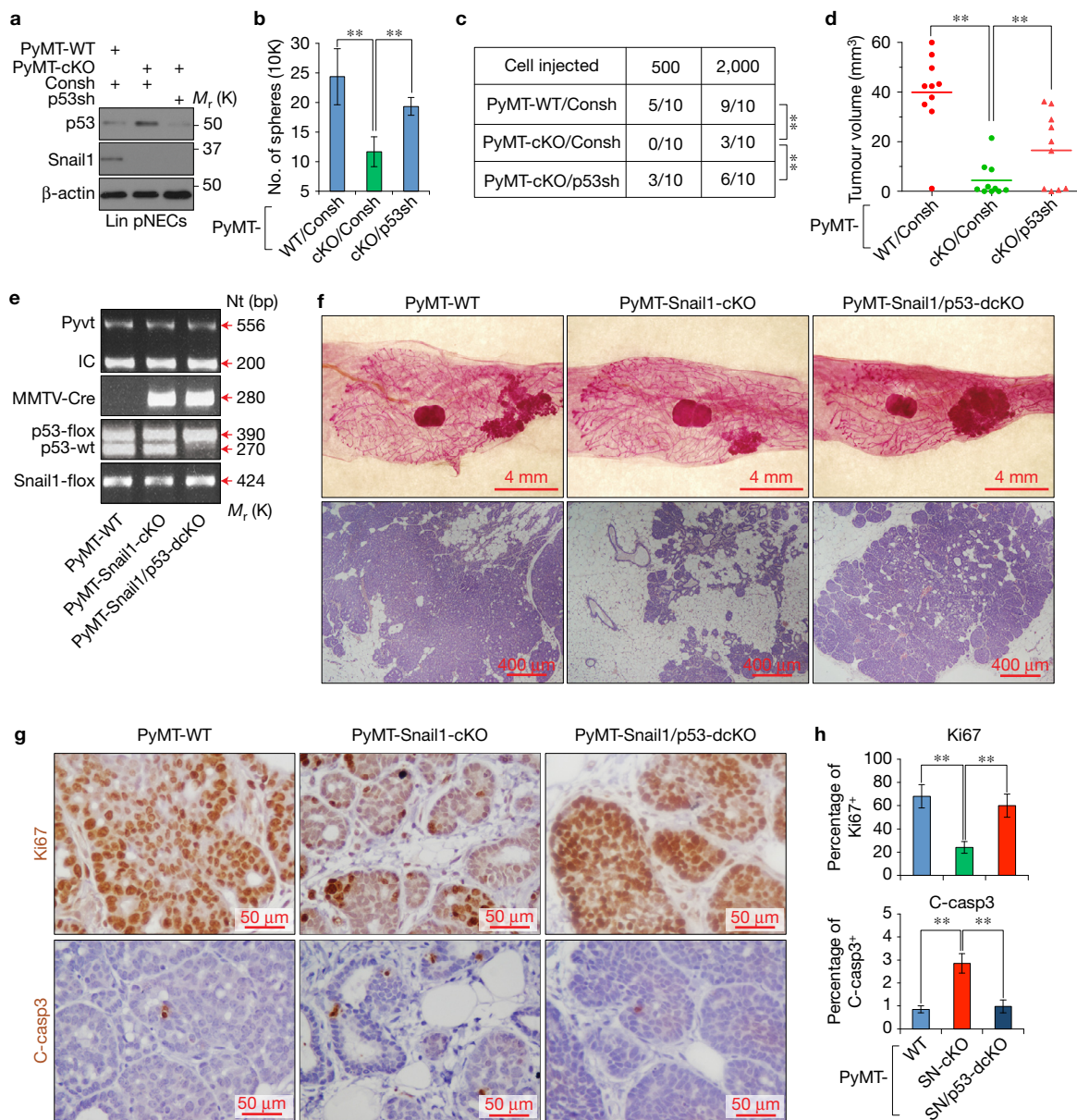


Figure 7 A Snail1/p53 axis regulates breast cancer tumorigenesis. (a) pNECs were isolated from mammary glands of 6-week-old PyMT-WT and -cKO mice, and transduced with pLKO.1 or pLKO.1-p53shRNA lentiviral vectors in suspension for 2 h. The transduced cells were cultured *in vitro* for 48 h, and cell lysates collected for immunoblotting to assess the efficiency of p53 knockdown. Results are representative of five independent experiments. (b) A portion of the transduced pNECs as described in a were subjected to tumoursphere formation assay. Data are presented as mean \pm s.e.m. ($n=5$ independent experiments). $**P<0.01$, one-way ANOVA test. (c,d) A portion of the transduced pNECs as described in a were subjected to *in vivo* tumorigenic assays wherein limiting dilutions of the cells were orthotopically injected into nude mouse recipients ($n=10$ mice, each). Tumour incidence (c) and volume (d) were measured 9 weeks post-injection. $**P<0.01$, Mann-Whitney test. (e) PCR results of the indicated genotypes. PyMT-WT: PyMT⁺/MMTV-Cre⁻/Snail1^{fl/fl}/p53^{fl/fl}; PyMT-SN-cKO: PyMT⁺/MMTV-Cre⁺/Snail1^{fl/fl}/p53^{wt/fl};

PyMT-SN/p53-dcKO: PyMT⁺/MMTV-Cre⁺/Snail1^{fl/fl}/p53^{fl/fl}. Arrows denote the expected PCR products. (f) Whole-mount carmine red staining (top panels) and H&E staining (bottom panels) of preneoplastic mammary gland from the indicated genotypes at seven weeks of age (images are representative of images from five mice). While PyMT-cKO display defects in early proliferative responses, the dual conditional deletion of Snail1 and p53 rescues tumour initiation. (g) Immunohistochemical staining of Ki67 and cleaved caspase 3 (C-casp3) in hyperplastic lesions of mammary glands from PyMT-WT, -Snail1-cKO and -Snail1/p53-dcKO mice at seven weeks of age (images are representative of images from five mice). (h) Quantification of Ki67- and C-casp3-positive cells (%) as shown in g. For quantification, 1,000 to 2,000 cells were counted in 10 random fields of each slide. Data are presented as mean \pm s.e.m. ($n=5$ independent experiments). $**P<0.01$, one-way ANOVA test. Unprocessed original scans of blots are shown in Supplementary Fig. 8. Source data are provided in Supplementary Table 1 (c).

represses tumoursphere-forming activity and tumorigenic potential *in vivo*, both activities are partially, but significantly, recovered by decreasing p53 levels (Fig. 7b-d). To directly assess the importance

of p53 as a Snail1 target during tumour initiation *in vivo*, we crossed MMTV-Cre transgenic mice with MMTV-PyMT-expressing animals carrying either floxed *Snail1* alleles alone or combined *Snail1* and *TP53*

floxed alleles (Fig. 7e). Remarkably, both the marked reduction in the proliferative activity and the increased pro-apoptotic activity of Snail1-cKO tumours are reversed following TP53 excision (Fig. 7f–h), thereby identifying p53 as a functionally critical Snail1 target *in vivo*.

DISCUSSION

Efforts to define roles for EMT-associated transcription factors in cancer have relied largely on model systems wherein Snail1 or related factors were purposefully over-expressed in transformed cell lines^{5,11–13}. Consequently, the ability and mechanisms by which endogenous Snail1 modulates tumour progression in the *in vivo* setting—and its relevance to human disease—remain largely undefined^{4,5,27–29,50,51}. Having noted an association between *Snail1*, wild-type *TP53* and disease progression in breast cancer patients, we used the MMTV-PyMT breast cancer model as a means to interrogate Snail1-wild-type p53 interactions *in vivo*. As recently reported, Snail1 is upregulated in tumour tissues of MMTV-PyMT mice^{8,9}, but using a β -galactosidase amplifying system, we find a far more global pattern of expression than that observed previously^{8,9}. Further, using a more efficient MMTV-Cre driver line than that used previously⁸, we find that *Snail1* excision markedly impairs the earliest phases of tumour growth and MaEC de-differentiation as well as the generation of TICs. A required role for Snail1 in tumour progression is likewise found to extend to the tumorigenic potential of aggressive adenocarcinomas. Snail1 appears to exert little effect on EMT programs, confirming reports that a complete loss of epithelial characteristics is rarely observed in the MMTV-PyMT model^{52,53}. Of note, Snail1 excision does not affect normal mammary gland development, a finding that dovetails recent work demonstrating that Snail1 expression is largely confined to the mammary gland stroma⁹. However, as Snail1 has recently been shown to modulate intestinal stem cell function⁵⁴, further studies, perhaps using more stem cell-specific Cre-drivers, are needed⁵⁵.

Other EMT-inducing transcription factors, including Slug and Twist, have been reported to directly or indirectly affect p53 function *in vitro*, but the outcome of these interactions has varied^{15–19,56–61}. Indeed, p53 has been reported to accelerate the proteasomal degradation of Snail1 or Slug^{18,56,61}. In our working model (Fig. 6n), binding interactions between Snail1 and p53 allow SNAG domain-associated HDAC1 to catalyse p53 deacetylation, thereby hastening the functional inactivation of p53. Hence, while most studies emphasize the role of Snail1-HDAC complexes in chromatin remodelling and transcriptional repression^{12,48,62}, we outline a previously unappreciated role for the deacetylase complex in controlling transcription factor function. Additional effects of Snail1 on the regulation of p300 acetylation as well as p53 transcriptional activity via its interaction with the p53 DNA-binding domain remain to be characterized, but we note that Snail1 can itself undergo acetylation⁶³ while Snail1 can also be recruited into p53-MDM2 complexes wherein MDM2 itself recruits HDAC1⁶⁴ (Supplementary Fig. 7i). These results support the existence of a more global-acting acetylation/deacetylation network that jointly controls both Snail1 and p53 function. Finally, it is important to stress that p53 function extends to diverse cellular responses, ranging from cell motility and invasion to the miRNA-dependent control of stem cell formation^{65–68}. As such, the Snail1-dependent regulation of p53 activity probably impacts multiple arms of the carcinoma phenotype. While recent studies have emphasized the ability of EMT-associated

transcription factors, including Snail1, to confer chemoresistance to neoplastic cell populations^{69,70}, our studies identify equally important, EMT-independent roles for Snail1 in regulating tumour progression. Given that most breast cancer patients express wild-type *TP53*, efforts aimed at modulating Snail1-p53 interactions *in vivo* may exert unexpected therapeutic benefit in this and other neoplastic states. □

METHODS

Methods, including statements of data availability and any associated accession codes and references, are available in the [online version of this paper](#).

Note: Supplementary Information is available in the online version of the paper

ACKNOWLEDGEMENTS

This research was supported by a grant from the Breast Cancer Research Foundation (BCRF) to S.J.W. as well as the Startup Fund from China Pharmaceutical University, the National Natural Science Foundation of China (NSFC 81572745 and 91539115), and the Jiangsu Province Innovative Research Team and State Key Laboratory of Natural Medicines (SKLNMZZJQ201604) to Z.-Q.W. Additional support was provided by the Changjiang Scholar and Innovative Research Team (IRT1193) to Q.-L.G. and the US National Institutes of Health (U01 CA180980) to X.S.L. We thank M.-D. Lai (China Pharmaceutical University, China) for critically reviewing this manuscript, W. Gu (Columbia University, USA) and P.-C. Yang (Academia Sinica, Taiwan) for providing HA-tagged p53 WT and mutant plasmids, R. Weinberg (Massachusetts Institute of Technology, USA) for sharing human mammary epithelial cells (HMLEs), A. Cano (Universidad Autonoma de Madrid, Spain) for Snail1 mutants, Y. Kang and L. Wan (Princeton University, USA) for sharing protocols of mouse mammary epithelial cell isolation, B. Gyorffy (Hungarian Academy of Sciences, Hungary) for assistance with the human breast cancer databases and R. Quick (University of Michigan, USA) for helpful discussions.

AUTHOR CONTRIBUTIONS

Z.-Q.W. and S.J.W. designed and supervised the project, analysed data, wrote the manuscript and approved the final version; T.N., X.-Y.L. and N.L. conducted experiments and analysed data. T.A., R.F., W.-C.L., Y.-W.Z., R.G.R., Y.-S.L., A.S. and T.F. conducted experiments. Z.-P.L., X.-J.X., X.-Q.Z., B.-A.C., X.S.L. and Q.-L.G. analysed data and provided relevant advice.

COMPETING FINANCIAL INTERESTS

The authors declare no competing financial interests.

Published online at <http://dx.doi.org/10.1038/ncb3425>

Reprints and permissions information is available online at www.nature.com/reprints

- Collado, M. & Serrano, M. Senescence in tumours: evidence from mice and humans. *Nat. Rev. Cancer* **10**, 51–57 (2010).
- Puisieux, A., Brabletz, T. & Caramel, J. Oncogenic roles of EMT-inducing transcription factors. *Nat. Cell Biol.* **16**, 488–494 (2014).
- Olivier, M., Hollstein, M. & Hainaut, P. TP53 mutations in human cancers: origins, consequences, and clinical use. *Cold Spring Harb. Perspect. Biol.* **2**, a001008 (2010).
- Moody, S. E. *et al.* The transcriptional repressor Snail promotes mammary tumor recurrence. *Cancer Cell* **8**, 197–209 (2005).
- Yook, J. I. *et al.* A Wnt-Axin2-GSK3 β cascade regulates Snail1 activity in breast cancer cells. *Nat. Cell Biol.* **8**, 1398–1406 (2006).
- Olmeda, D. *et al.* SNAI1 is required for tumor growth and lymph node metastasis of human breast carcinoma MDA-MB-231 cells. *Cancer Res.* **67**, 11721–11731 (2007).
- Zhang, K. *et al.* The collagen receptor discoidin domain receptor 2 stabilizes Snail1 to facilitate breast cancer metastasis. *Nat. Cell Biol.* **15**, 677–687 (2013).
- Tran, H. D. *et al.* Transient Snail1 expression is necessary for metastatic competence in breast cancer. *Cancer Res.* **74**, 6330–6340 (2014).
- Ye, X. *et al.* Distinct EMT programs control normal mammary stem cells and tumour-initiating cells. *Nature* **525**, 256–260 (2015).
- Mani, S. A. *et al.* The epithelial-mesenchymal transition generates cells with properties of stem cells. *Cell* **133**, 704–715 (2008).
- Nieto, M. A. Epithelial plasticity: a common theme in embryonic and cancer cells. *Science* **342**, 1234850 (2013).
- Tam, W. L. & Weinberg, R. A. The epigenetics of epithelial-mesenchymal plasticity in cancer. *Nat. Med.* **19**, 1438–1449 (2013).
- Gyorffy, B. *et al.* An online survival analysis tool to rapidly assess the effect of 22,277 genes on breast cancer prognosis using microarray data of 1,809 patients. *Breast Cancer Res. Treat.* **123**, 725–731 (2010).

14. Gyorffy, B. *et al.* TP53 mutation-correlated genes predict the risk of tumor relapse and identify MPS1 as a potential therapeutic kinase in TP53-mutated breast cancers. *Mol. Oncol.* **8**, 508–519 (2014).
15. Kajita, M., McClinic, K. N. & Wade, P. A. Aberrant expression of the transcription factors Snail and Slug alters the response to genotoxic stress. *Mol. Cell Biol.* **24**, 7559–7566 (2004).
16. Escrava, M. *et al.* Repression of PTEN phosphatase by Snail1 transcriptional factor during γ radiation-induced apoptosis. *Mol. Cell Biol.* **28**, 1528–1540 (2008).
17. Lee, S. H. *et al.* Blocking of p53-Snail binding, promoted by oncogenic K-Ras, recovers p53 expression and function. *Neoplasia* **11**, 22–31 (2009).
18. Lim, S. O., Kim, H. & Jung, G. p53 inhibits tumor cell invasion via the degradation of Snail protein in hepatocellular carcinoma. *FEBS Lett.* **584**, 2231–2236 (2010).
19. Perez-Mancera, P. A. *et al.* Cancer development induced by graded expression of Snail in mice. *Hum. Mol. Genet.* **14**, 3449–3461 (2005).
20. Rowe, R. G. *et al.* Mesenchymal cells reactivate Snail1 expression to drive three-dimensional invasion programs. *J. Cell Biol.* **184**, 399–408 (2009).
21. Lin, Y. *et al.* Snail1-dependent control of embryonic stem cell pluripotency and lineage commitment. *Nat. Commun.* **5**, 3070 (2014).
22. Wu, Z. Q. *et al.* A Snail1/Notch1 signalling axis controls embryonic vascular development. *Nat. Commun.* **5**, 3998 (2014).
23. Grande, M. T. *et al.* Snail1-induced partial epithelial-to-mesenchymal transition drives renal fibrosis in mice and can be targeted to reverse established disease. *Nat. Med.* **21**, 989–997 (2015).
24. Guy, C. T., Cardiff, R. D. & Muller, W. J. Induction of mammary tumors by expression of polyomavirus middle T oncogene: a transgenic mouse model for metastatic disease. *Mol. Cell Biol.* **12**, 954–961 (1992).
25. Lin, E. Y. *et al.* Progression to malignancy in the polyoma middle T oncoprotein mouse breast cancer model provides a reliable model for human diseases. *Am. J. Pathol.* **163**, 2113–2126 (2003).
26. Cheung, K. J., Gabrielson, E., Werb, Z. & Ewald, A. J. Collective invasion in breast cancer requires a conserved basal epithelial program. *Cell* **155**, 1639–1651 (2013).
27. Geradts, J. *et al.* Nuclear Snail1 and nuclear ZEB1 protein expression in invasive and intraductal human breast carcinomas. *Hum. Pathol.* **42**, 1125–1131 (2011).
28. Wu, Z. Q. *et al.* Canonical Wnt signaling regulates Slug activity and links epithelial-mesenchymal transition with epigenetic Breast Cancer 1, Early Onset (BRCA1) repression. *Proc. Natl Acad. Sci. USA* **109**, 16654–16659 (2012).
29. Muenst, S. *et al.* Nuclear expression of Snail is an independent negative prognostic factor in human breast cancer. *Dis. Markers* **35**, 337–344 (2013).
30. Wagner, K. U. *et al.* Spatial and temporal expression of the Cre gene under the control of the MMTV-LTR in different lines of transgenic mice. *Transgenic Res.* **10**, 545–553 (2001).
31. Jiao, B. *et al.* Paternal RLIM/Rnf12 is a survival factor for milk-producing alveolar cells. *Cell* **149**, 630–641 (2012).
32. Chen, Q. *et al.* A temporal requirement for Hippo signaling in mammary gland differentiation, growth, and tumorigenesis. *Genes Dev.* **28**, 432–437 (2014).
33. Shackleton, M. *et al.* Generation of a functional mammary gland from a single stem cell. *Nature* **439**, 84–88 (2006).
34. Asselin-Labat, M. L. Gata-3 is an essential regulator of mammary-gland morphogenesis and luminal-cell differentiation. *Nat. Cell Biol.* **9**, 201–209 (2007).
35. Kouros-Mehr, H. *et al.* GATA-3 links tumor differentiation and dissemination in a luminal breast cancer model. *Cancer Cell* **13**, 141–152 (2008).
36. Wan, L. *et al.* MTDH-SND1 interaction is crucial for expansion and activity of tumor-initiating cells in diverse oncogene- and carcinogen-induced mammary tumors. *Cancer Cell* **26**, 92–105 (2014).
37. Malanchi, I. *et al.* Interactions between cancer stem cells and their niche govern metastatic colonization. *Nature* **481**, 85–89 (2011).
38. Thiery, J. P., Acloque, H., Huang, R. Y. & Nieto, M. A. Epithelial-mesenchymal transitions in development and disease. *Cell* **139**, 871–890 (2009).
39. Dong, C. *et al.* Loss of FBP1 by Snail-mediated repression provides metabolic advantages in basal-like breast cancer. *Cancer Cell* **23**, 316–331 (2013).
40. Ota, I., Li, X. Y., Hu, Y. & Weiss, S. J. Induction of a MT1-MMP and MT2-MMP-dependent basement membrane transmigration program in cancer cells by Snail1. *Proc. Natl Acad. Sci. USA* **106**, 20318–20323 (2009).
41. Anisneau, S. *et al.* Induction of EMT by Twist proteins as a collateral effect of tumor-promoting inactivation of premature senescence. *Cancer Cell* **14**, 79–89 (2008).
42. Pyun, B. J. *et al.* Mutual regulation between DNA-PKcs and Snail1 leads to increased genomic instability and aggressive tumor characteristics. *Cell Death Dis.* **4**, e517 (2013).
43. Kang, G. Y. *et al.* Inhibition of Snail1-DNA-PKcs protein-protein interface sensitizes cancer cells and inhibits tumor metastasis. *J. Biol. Chem.* **288**, 32506–32516 (2013).
44. Tang, Y., Zhao, W., Chen, Y., Zhao, Y. & Gu, W. Acetylation is indispensable for p53 activation. *Cell* **133**, 612–626 (2008).
45. Thompson, P. R. *et al.* Regulation of the p300 HAT domain via a novel activation loop. *Nat. Struct. Mol. Biol.* **11**, 308–315 (2004).
46. Ferreon, J. C. *et al.* Cooperative regulation of p53 by modulation of ternary complex formation with CBP/p300 and HDM2. *Proc. Natl Acad. Sci. USA* **106**, 6591–6596 (2009).
47. Villarejo, A., Cortes-Cabrera, A., Molina-Ortiz, P., Portillo, F. & Cano, A. Differential role of Snail1 and Snail2 zinc fingers in E-cadherin repression and epithelial to mesenchymal transition. *J. Biol. Chem.* **289**, 930–941 (2014).
48. Peinado, H., Ballestar, E., Esteller, M. & Cano, A. Snail mediates E-cadherin repression by the recruitment of the Sin3A/histone deacetylase 1 (HDAC1)/HDAC2 complex. *Mol. Cell Biol.* **24**, 306–319 (2004).
49. Choi, S. *et al.* Structural basis for the selective nuclear import of the C2H2 zinc-finger protein Snail by importin beta. *Acta Crystallogr. D Biol. Crystallogr.* **70**, 1050–1060 (2014).
50. Vincent, T. *et al.* A Snail1-SMAD3/4 transcriptional repressor complex promotes TGF- β mediated epithelial-mesenchymal transition. *Nat. Cell Biol.* **11**, 943–950 (2009).
51. Blanco, M. J. *et al.* Correlation of Snail expression with histological grade and lymph node status in breast carcinomas. *Oncogene* **21**, 3241–3246 (2002).
52. Trimboli, A. J. *et al.* Direct evidence for epithelial-mesenchymal transitions in breast cancer. *Cancer Res.* **68**, 937–945 (2008).
53. Lan, L. *et al.* Shp2 signaling suppresses senescence in PyMT-induced mammary gland cancer in mice. *EMBO J.* **34**, 1493–1508 (2015).
54. Horvay, K. *et al.* Snail1 regulates cell lineage allocation and stem cell maintenance in the mouse intestinal epithelium. *EMBO J.* **34**, 1319–1335 (2015).
55. Wang, D. *et al.* Identification of multipotent mammary stem cells by protein C receptor expression. *Nature* **517**, 81–84 (2015).
56. Kim, J. *et al.* Cooperative actions of p21WAF1 and p53 induce Slug protein degradation and suppress cell invasion. *EMBO Rep.* **15**, 1062–1068 (2014).
57. Piccinin, S. *et al.* A 'Twist box' code of p53 inactivation: Twist box: p53 interaction promotes p53 degradation. *Cancer Cell* **22**, 404–415 (2012).
58. Shiota, M. *et al.* Twist and p53 reciprocally regulate target genes via direct interaction. *Oncogene* **27**, 5543–5553 (2008).
59. Beck, B. *et al.* Different levels of Twist1 regulate skin tumor initiation, stemness, and progression. *Cell Stem Cell* **16**, 67–79 (2015).
60. Gajula, R. P. *et al.* The Twist box domain is required for Twist1-induced prostate cancer metastasis. *Mol. Cancer Res.* **11**, 1387–1400 (2013).
61. Wang, S. P. *et al.* p53 controls cancer cell invasion by inducing the MDM2-mediated degradation of Slug. *Nat. Cell Biol.* **11**, 694–704 (2009).
62. Lamouille, S., Xu, J. & Derynck, R. Molecular mechanisms of epithelial-mesenchymal transition. *Nat. Rev. Mol. Cell Biol.* **15**, 178–196 (2014).
63. Hsu, D. S. *et al.* Acetylation of Snail modulates the cytokinome of cancer cells to enhance the recruitment of macrophages. *Cancer Cell* **26**, 534–548 (2014).
64. Ito, A. *et al.* MDM2-HDAC1-mediated deacetylation of p53 is required for its degradation. *EMBO J.* **21**, 6236–6245 (2002).
65. Gadea, G., de Toledo, M., Anguille, C. & Roux, P. Loss of p53 promotes RhoA-ROCK-dependent cell migration and invasion in 3D matrices. *J. Cell Biol.* **178**, 23–30 (2007).
66. Godar, S. *et al.* Growth-inhibitory and tumor-suppressive functions of p53 depend on its repression of CD44 expression. *Cell* **134**, 62–73 (2008).
67. Mak, A. S. p53 in cell invasion, podosomes, and invadopodia. *Cell Adhes. Migr.* **8**, 205–214 (2014).
68. Chang, C. J. *et al.* p53 regulates epithelial-mesenchymal transition and stem cell properties through modulating miRNAs. *Nat. Cell Biol.* **13**, 317–323 (2011).
69. Fischer, K. R. *et al.* Epithelial-to-mesenchymal transition is not required for lung metastasis but contributes to chemoresistance. *Nature* **527**, 472–476 (2015).
70. Zheng, X. *et al.* Epithelial-to-mesenchymal transition is dispensable for metastasis but induces chemoresistance in pancreatic cancer. *Nature* **527**, 525–530 (2015).

METHODS

Transgenic mouse strains and tumour monitoring. Transgenic mice were housed under standard specific-pathogen-free (SPF) conditions and all research involving animals strictly complied with protocols approved by the Animal Welfare and Ethics Committee (AWEC, China Pharmaceutical University), and the University Committee on Use and Care of Animals (UCUCA, University of Michigan). Mice carrying Snail1 (exon 3) floxed alleles and mice with Snail1-LacZ knock-in alleles have been described previously^{20–22}. MMTV-PyMT (stock No. 002374), ROSA26-LacZ (stock No. 003474) and p53^{fl/fl} (stock No. 008652) transgenic mice were purchased from Jackson Laboratory. MMTV-Cre (line F, stock No. 01XA9) mice were obtained from NCI-Frederick. All mice were on a mixed FVB/C57BL6 background with littermate controls (females) used in all experiments. For spontaneous tumorigenesis studies, weaned females were examined twice a week for the development of mammary tumours by palpation. For metastasis studies, lungs were collected for analysis at 9 weeks post initial detection of palpable tumours, and metastatic nodules counted. The maximal tumour sizes permitted under the approved protocols are 3 cm (length) × 3 cm (width). The investigators were not blinded to allocation during experiments and outcome assessment. No method of randomization was used as mice were segregated into groups based on genotype alone. No statistical method was used to predetermine sample size.

Isolation of Lin⁻ NECs and pNECs and flow cytometry analysis. Isolation of pNECs and NECs was performed as described previously with slight modifications²⁶. Briefly, preneoplastic glands or primary tumours were dissected into pieces and dissociated enzymatically at 37 °C for 1 h in culture medium (DMEM/F12) containing 5% FBS, 10 ng ml⁻¹ EGF, 500 ng ml⁻¹ hydrocortisone, 5 mg ml⁻¹ insulin, 20 ng ml⁻¹ cholera toxin and 1% penicillin/streptomycin supplemented with collagenase/hyaluronidase (STEMCELL Technologies). Organoids were harvested and incubated with 0.25% trypsin-EDTA for 2 min, 5 mg ml⁻¹ Dispase plus 0.1 mg ml⁻¹ DNase (Invitrogen) for 5 min, and 0.64% NH₄Cl for 5 min at 37 °C. Following filtration through a 40 µm cell strainer, cells were harvested and resuspended in HBSS buffer supplemented with 0.5% BSA. For flow cytometry, single-cell suspensions were incubated with an antibody cocktail containing CD31, CD45 and Ter119 (STEMCELL Technologies, catalogue No. 19757C.1), a secondary biotin-labelled antibody cocktail (STEMCELL Technologies, catalogue No. 19153), and magnetic beads (15 min each) on ice (STEMCELL Technologies, catalogue No. 19150). The unbound cells were collected and the bound cells discarded. Purified cells were labelled with FITC-CD24 (BD Biosciences, catalogue No. 561777, clone No. M1/69, 1:800) or APC-CD24 (BD Biosciences, catalogue No. 562349, clone No. M1/69, 1:800), PE-CD29 (BD Biosciences, catalogue No. 562801, clone No. HM β1-1, 1:400) or Alexa Fluor 488-CD29 (BioLegend, catalogue No. 102212, clone No. HM β1-1, 1:400), PE-CD61 (BD Biosciences, catalogue No. 561910, clone No. HM β3-1, 1:400) or APC-CD61 (BioLegend, catalogue No. 104316, clone No. HM β3-1, 1:400), or FITC-CD90 (BioLegend, catalogue No. 105306, clone No. 30-H12, 1:200) for 30 min, followed by DAPI staining for 5 min before FACS analysis. All conjugated primary antibodies used for flow cytometry analysis were purchased from BioLegend. In some experiments, ALDH activity of purified cells was measured using a kit from StemCELL Technologies according to the manufacturer's instructions.

Cell culture. All cell lines were purchased from ATCC. 293T, MCF-7 and MDA-MB-231 cells were grown in DMEM. ZR75-1 and CAMA-1 cells were grown in RPMI-1640 and EMEM, respectively. Culture medium was supplemented with 10% heat-inactivated fetal bovine serum and 1% penicillin/streptomycin (all from Invitrogen). Cells were tested for mycoplasma contamination every 2 weeks, and only mycoplasma-negative cells were used. No cell lines in this study were authenticated in our laboratory. No cell lines used in this study were found in the database of commonly misidentified cell lines that is maintained by ICLAC and NCBI Biosample.

Tumorigenesis assay. Nude mice were housed under standard SPF conditions and the animal experiments strictly complied with protocols approved by the Animal Welfare and Ethics Committee (AWEC, China Pharmaceutical University), and the University Committee on Use and Care of Animals (UCUCA, University of Michigan). Fifty microlitres of 1:1 PBS and Matrigel (BD Biosciences) mixture of preneoplastic and neoplastic mammary epithelial cells (pNECs and NECs) at limiting dilutions were transplanted into the fourth mammary glands of 4-week-old nude mice. Mice were examined twice a week for the development of tumours by palpation, and tumour volumes calculated at 7 or 9 weeks after transplantation using the formula $V = \pi \times \text{length} \times \text{width}^2 / 6$. The investigators were not blinded to allocation during experiments and outcome assessment. Mice were randomly allocated to each group by an independent person in the laboratory. No statistical method was used to predetermine sample size.

Mammosphere assay. Single cells were plated in ultralow-attachment plates (Corning) with serum-free DMEM/F12 medium (Invitrogen), supplemented with B27 (Invitrogen), 20 ng ml⁻¹ EGF, 20 ng ml⁻¹ basic fibroblast growth factor (R & D Systems), and 4 mg ml⁻¹ heparin (Sigma). Mammospheres were counted 7 days after plating. In some cases, mammospheres were trypsinized and the cells were re-seeded in ultralow-attachment plates.

Whole-mount analysis and immunohistochemistry. For whole-mount analysis, the fourth inguinal mammary glands were dissected and fixed in Carnoy's solution, followed by hydration and carmine red staining. The stained glands were then flattened, dehydrated and mounted. For histology, 4% paraformaldehyde (PFA) fixed tissues were embedded in paraffin and sectioned, followed by haematoxylin and eosin (H&E) staining. For immunohistochemical analysis, paraffin-embedded sections were deparaffinized, rehydrated and subjected to antigen heat retrieval with citric buffer (pH 6.0). The sections were incubated in blocking buffer (5% goat serum in PBS) containing primary antibodies against K14 (BioLegend, catalogue No. 905301, 1:200), p-ATM (Ser1981; Millipore, catalogue No. MAB3806, clone No. 10H11.E12, 1:100), γ-H2AX (Ser139; Cell Signaling, catalogue No. 9718, clone No. 20E3, 1:100), cleaved caspase 3 (Cell Signaling, catalogue No. 9664, clone No. 5AE1, 1:100), Ki67 (Abcam, catalogue No. ab15580, 1:1,000), p-Histone H3 (Cell Signaling, catalogue No. 9701, 1:400), p53 (Vector Laboratories, catalogue No. VP-P956, 1:500), and p-Rb (Cell Signaling, catalogue No. 9308, 1:200), followed by incubation with biotinylated goat anti-mouse and goat anti-rabbit secondary antibodies (Vector Laboratories, 1:200). Standard ABC kit and DAB (Vector Laboratories) were used for the detection of HRP activity. Slides were counterstained with haematoxylin, dehydrated and mounted. In some experiments, sections or cultured cells were incubated with primary antibodies against β-casein (Santa Cruz, catalogue No. sc-30442, 1:200), vimentin (Cell Signaling, catalogue No. 5741, clone No. D21H3, 1:200), E-cadherin (BD, catalogue No. 610181, clone No. 36/E-cadherin, 1:1,000), K14 (BioLegend, catalogue No. 905301, 1:100), p53 (Cell Signaling, catalogue No. 2524, clone No. 1C12, 1:200), Pan-AcK (Cell Signaling, catalogue No. 9441, 1:200) and cleaved caspase 3 (Cell Signaling, catalogue No. 9664, clone No. 5A1E, 1:100), followed by incubation with goat anti-mouse Alexa 594 and goat anti-rabbit Alexa 488 secondary antibodies (Invitrogen, 1:400) and DAPI (Invitrogen).

X-gal staining. To detect βGal/LacZ activity, the dissected fourth inguinal mammary glands, primary tumours or frozen sections were fixed in fixative solution (containing 4% formaldehyde, 0.5% glutaraldehyde, 1.25 mM EGTA, 2 mM MgCl₂, 0.1 M sodium phosphate, pH 7.2), washed in rinse buffer (containing 2 mM MgCl₂, 0.2% deoxycholate, 0.2% NP-40, 0.1 M sodium phosphate, pH 7.2) and incubated overnight in X-gal staining buffer (containing 2 mM MgCl₂, 0.2% deoxycholate, 0.2% NP-40, 1 mg ml⁻¹ X-gal, 5 mM potassium ferrocyanide, 5 mM potassium ferricyanide, 0.1 M sodium phosphate, pH 7.2). After being stained, whole-mount tissues were washed with PBS, transferred to 70% alcohol and then viewed under a Leica dissecting microscope. Frozen-sectioned tissues were washed with PBS, dehydrated in series of alcohol baths and mounted.

Cloning, virus production and infection. Wild-type p3× FLAG-Snail1 vector was generated and used as described previously²⁸. To generate FLAG-tagged Snail1 truncation mutants, indicated fragments were amplified by PCR and subcloned into a p3× FLAG-CMV vector (Sigma, catalogue No. E7533). To generate HA-tagged Snail1 ΔSNAG mutant, the indicated fragment together with NH₂-terminal HA was amplified by PCR and subcloned into a pcDNA3.1 vector (Invitrogen, catalogue No. V79020). To generate lentiviral vector expressing Snail1, full-length Snail1 gene was amplified by PCR and subcloned into a pLenti-Lox-IRES vector (Vector Core of University of Michigan). To generate pLKO.1-p53shRNA, forward oligonucleotide 5'-CCGGAATGCCCCAGGGAGCGCAACTCGAGTTGCGCTCCCTGGGGG CAGTTTTTTTG-3' was annealed with reverse oligonucleotide 5'-AATTCAAAAA AAACGCCCCAGGGAGCGCAACTCGAGTTGCGCTCCCTGGGGGAGAGT T-3', and the annealed oligonucleotides were subcloned into an AgeI/EcoRI (NEB, catalogue No. R0552S and R0101S) digested pLKO.1-TRC cloning vector (Addgene, catalogue No. 10879). HA-tagged p53 wild type as well as truncated mutants were provided by P.-C. Yang (Academia Sinica, Taiwan)⁶¹. HA-ubiquitin (catalogue No. 18712), GFP-p53 (catalogue No. 12091), GST-p53 (catalogue No. 10852), psPAX2 (catalogue No. 12260), pMD2.G (catalogue NO. 12259), pRSV-Rev (catalogue NO. 12253), pMDLg/pRRE (catalogue NO. 12251), pCMV-VSV-G (catalogue NO. 8454) and pLKO.1-GFPshRNA (catalogue No. 30323) were purchased from Addgene. Recombinant adenovirus expressing βGal or Cre was purchased from the Vector Core of University of Michigan. For infection of attached cells, target cells were incubated in complete medium supplemented with adenoviral particles (MOI = 50) for 24 h, refed with fresh medium containing viral particles (MOI = 50) and further cultured for another 24 h. Cells were collected for further use. For infection of cell suspensions, target cells in suspension were infected with adenoviral particles (MOI = 100) and centrifuged for 2 h at room temperature. Cells were harvested

for further use. Production and infection of lentiviral particles were performed as described previously²². Briefly, to produce pLKO.1 lentiviral particles, 293T cells were co-transfected with pLKO.1-GFPshRNA (or pLKO.1-mp53shRNA), psPAX2 and pMD2.G at a ratio of 4:3:1. Cells were fed with fresh medium 24 h post transfection, and conditioned medium containing viral particles was harvested 48 h and 72 h post transfection. To produce pLenti-Lox-IRES lentiviral particles, 293T cells were co-transfected with pLenti-Lox-IRES (or pLL-Snail1), pRSV-Rev, pMDLg/pRRE and pCMV-VSV-G at a ratio of 1:1:1:1. Cells were fed with fresh medium 24 h post transfection, and conditioned medium containing viral particles was harvested 48 h and 72 h post transfection. Viral particles were stored at -80°C for further use or immediately used. For infection of attached cells, target cells were incubated with a mixture of conditioned medium (containing viral particles) and culture medium at a ratio of 1:1 for 24 h in the presence of $8\ \mu\text{g ml}^{-1}$ Polybrene (Sigma). Cells were re-infected with viral particles for another 24 h and harvested for further use. For infection of cell suspensions, target cells were suspended in culture medium supplemented with an equal amount of conditioned medium (containing viral particles) and centrifuged for 2 h at room temperature. Cells were harvested for further use.

Immunoprecipitation and immunoblotting. Cultured pNECs and NECs were infected with adenoviral vectors expressing recombinant βGal or Cre, and the cell lysates were prepared and subjected to immunoblot assay using antibodies against Snail1 (Cell Signaling, catalogue No. 3895, clone No. L70G2, 1:1,000), Ac-p53 (Lys379, Cell Signaling, catalogue No. 2570, 1:500), Ac-p300 (K1499, Cell Signaling, catalogue No. 4771, 1:500), GFP (Invitrogen, catalogue No. A-11122, 1:5,000), HDAC1 (Cell Signaling, catalogue No. 5356, clone No. 10E2, 1:1,000), HDAC1 (Cell Signaling, catalogue No. 2062, clone No. 10E2, 1:1,000), p16 (Abcam, catalogue No. ab54210, clone No. 2D9A12, 1:1,000), $\gamma\text{-H2AX}$ (Ser139; Cell Signaling, catalogue No. 9718, clone No. 20E3, 1:500), p21 (Abcam, catalogue No. ab7903, clone No. WA-1, 1:200), p-ATM (Ser1981; Millipore, catalogue No. 905301, clone No. 10H11.E12, 1:500), MDM2 (Millipore, catalogue No. 04-1530, clone No. 3G9, 1:200) and $\beta\text{-actin}$ (Sigma, catalogue No. A5316, clone No. AC-74, 1:10,000). For immunoprecipitation (IP) assay in PyMT-induced carcinoma cells, control and Snail1-deleted NECs were incubated with anti-Pan-Ack (Cell Signaling, catalogue No. 9441, 1:300), followed by incubation with pre-cleared Protein A (or G) agarose beads (Santa Cruz). The immunocomplexes were resolved by 4–20% (vol/vol) SDS-PAGE and subjected to immunoblot assay using the indicated antibodies. For IP assay in 293T cells, FLAG-Snail1 (WT or truncated mutants) together with GFP-p53, or HA-p53 (WT or truncated mutants) together with FLAG-Snail1 were co-transfected into the cells. Cell lysates were incubated with anti-GFP (Invitrogen, catalogue No. A-11122, 1:500), anti-FLAG-M2 (Sigma, catalogue No. F3165, clone No. M2, 1:500) or anti-HA (Clontech, catalogue No. 631207, 1:500), followed by immunoblotting using the indicated antibodies.

qRT-PCR assay. Total RNAs ($1.0\ \mu\text{g}$) from cultured or freshly isolated single cells were extracted using the RNeasy kit (Qiagen, catalogue No. 74104) and reverse transcribed with the SuperScript III cDNA Synthesis kit (Invitrogen, catalogue No. 18080051) according to the manufacturer's instructions. qPCR was performed using the SYBR Green PCR Master Mix (Applied Biosystems, catalogue No. 4368577), and relative mRNA expression was normalized to GAPDH. PCR primers for amplifying the indicated mouse genes are used as follows: *Snail1*-5'-AAGATGCACATCCGAAGC-3'/5'-ATCTCTTACATCCGAGTGG-3', *Slug*-5'-CTCCAGACCCTGGCTGCTTCA-3'/5'-GTCTGCAGATGTGCCCTCAGG3-', *Csn1s1*-5'-CCAGTGCACCCTGGAAACAGCT-3'/5'-GGGAAGCTTGCTGTACCAGGG-3', *Csn1s2a*-5'-GCAACCTTCCACCAGCAGC-3'/5'-GCTGATGGATTCTGGGTGGG-3', *Csn2*-5'-CCTTGTGGCCCTTGCTCTTGC-3'/5'-GGCTGTGACTGGATCTGGAG-3', *Car3*-5'-CACTGGGGCTCCTCTGATGAC-3'/5'-GGCTGCTCAGAGCCTCTCA-3', *Car6*-5'-CTGGAACTCAGCGGCTCTGA-3'/5'-CGCTAACACAGCT

AGGCCGT-3', *Fabp4*-5'-CACCGCAGACGACAGGAAGGT-3'/5'-CCATCCCAC TTCTGCACCTGC-3', *Lalba*-5'-GTGAGTTCCCCGAGTCGGAGA-3'/5'-GGGCT TCTCACAACGCCACTG-3', *Wap*-5'-CCATGTGCTGTCCCGTTCTCT-3'/5'-CA CGGCCCGGTACTACTGATC-3', *Cdh1*-5'-GAAGTCCATGGGGCACCACCA-3 '/5'-CTGAGACCTGGGTACACGCTG-3', *Vim*-5'-AGCGTGGCTGCCAAGAAC CTC-3'/5'-GCAGGGCATCGTTGTTCCGGT-3', *Fhl1*-5'-GGGTGACACTTATGA GCGCC-3'/5'-GACTGACCCCTTCATGGCAG-3', *p53*-5'-AGCTCCCTCTGA GCCAGGAGA-3'/5'-TCCTCAACATCCTGGGGCAGC-3', *p21*-5'-TGCCGTGT CTCTTCGGTCCC-3'/5'-TAGACCTGGGCAGCCCTAGG-3', *Mdm2*-5'-CGCT GAGTGAGAGCAGACGTC-3'/5'-GCTCCCCAGGTAGCTCATCTG-3', *p16*-5'-AGCTGCGCTCTGGCTTTCGTG-3'/5'-GCTGCTACGTGAACGTTGCC-3'.

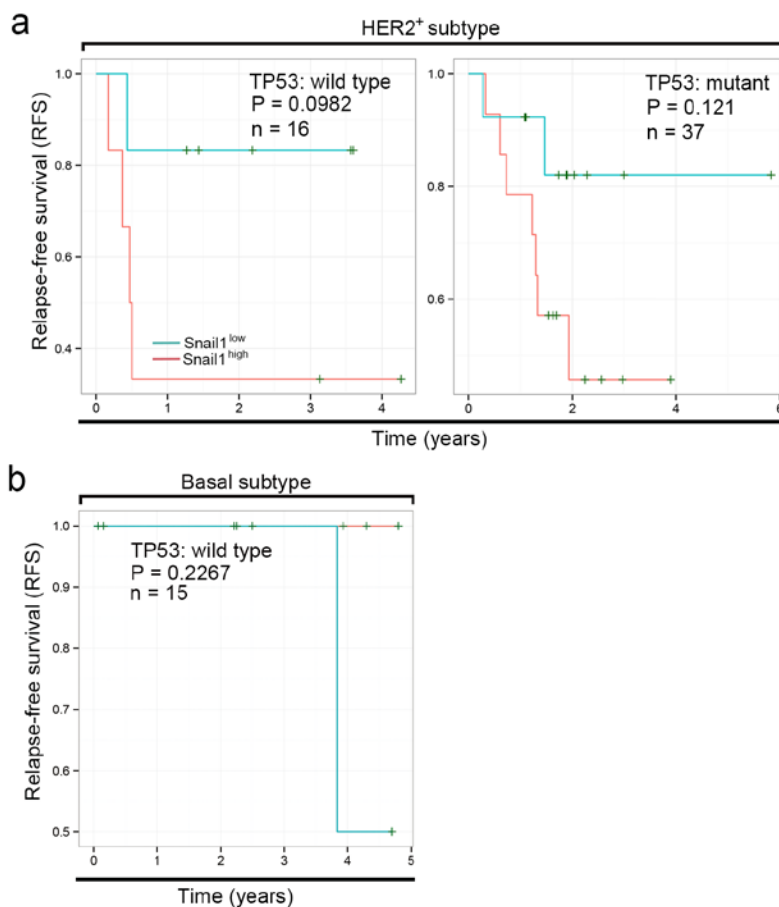
Genotyping. Transgenic mouse tails were cut ($\sim 2\ \text{mm}$) and digested at 95°C for 30 min in 50 μl of buffer 1 (containing 10 N NaOH and 0.5 M EDTA, pH 12.0). An equal amount of buffer 2 (containing 40 mM Tris-HCl, pH 5.0) was added to neutralize buffer 1. The mixtures were immediately vortexed and centrifuged at 12,000g for 5 min. The supernatants (tail genomic DNA) were collected and stored in -20°C for further use. For genotyping, 1 μl of extracted genomic DNA was used as a template in 20 μl of PCR reaction mixture containing 10 μl 2 \times GoTaq GreenMaster Mix (Promega, catalogue No. M7123), 0.5 μl forward/reverse primers and 8.5 μl H_2O . PCR primers for amplifying the indicated mouse transgenes are used as follows: *PyMT*-5'-GGAAGCAAGTACTTCAACAAGG-3'/5'-GGAAAGTCACTAGGAG CAGGG-3', *PyMT Internal control*-5'-CAAATGTTGCTTGTCTGGT-3'/5'-GTC AGTCGAGTGCACAGTTT-3', *Rosa-LacZ*-5'-GCGAAGAGTTTGTCTCAACC-3'/5'-AAAGTCGCTCTGAGTTGTTAT-3'/5'-GGAGCGGGAGAAATGGATATG-3', *MMTV-Cre*-5'-GGTTCTGATCTGAGCTCTGAGTG-3'/5'-CATCACTCGTT GGATCGACCGG-3', *Snail1-LacZ*-5'-GCAGCCTCTGTTCCACATACACTTCA-3'/5'-GTCTGTTGACTCTCAAAGAAGGTGGC-3', *Snail1-flox*-5'-CTGCCAGGT GGGAAAGGACT-3'/5'-CAAGGACATGCGGGGAGAAGGT-3', *p53-flox*-5'-GGTT AAACCCAGTTGACA-3'/5'-GGAGGCAGAGACAGTTGGAG-3'.

Clinical data analysis. Patient data were collected from the following databases: E-MTAB-365 (239 samples), E-TABM-43 (37 samples), GSE16446 (68 samples), GSE22093 (65 samples) and GSE3494 (251 samples). Samples were divided as 'high' and 'low' groups by the median of Snail1 expression. Survival was fitted by the 'survfit' function, and Kaplan-Meier curves were drawn by the 'ggsurv' function in the R package 'survival'. Differences between two survival curves were measured by the G-rho family of tests.

Statistics and reproducibility. Data are presented as mean \pm s.e.m. Statistical analysis was performed as described in each corresponding figure legend. Sample sizes are shown in each corresponding figure legend. $P < 0.05$ is considered significant.

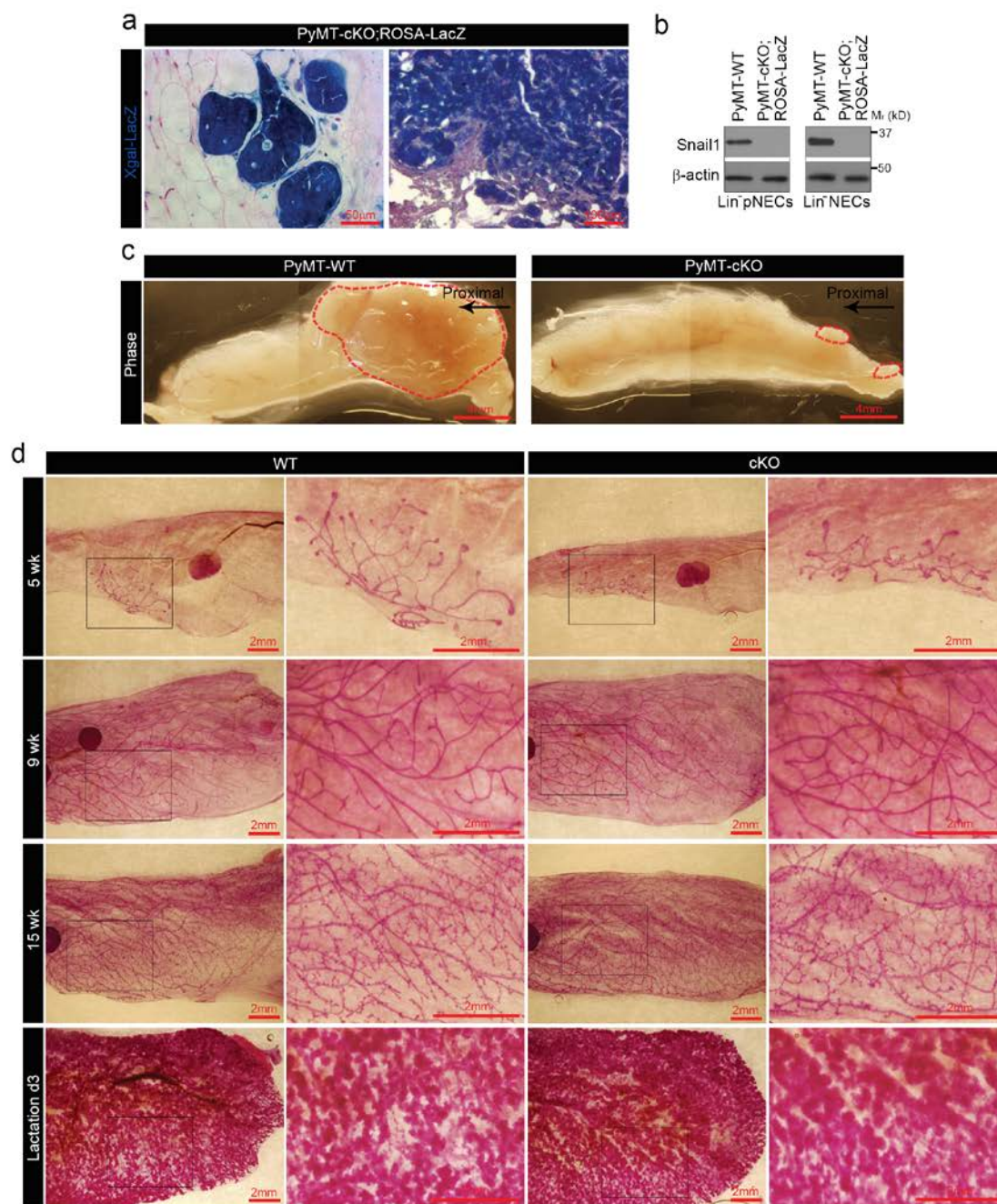
Representative figures are shown in Figs 1f,g, 2a–d,f, 3a,c,g,h,j,k, 4a,b,d, 5a–d,f, 6a–e,g,i–m and 7a,c–g and Supplementary Figs 2a–d, 3b, 4a,b, 5a,c,e,f,h, 6a,c–e,g and 7b–i. The experiments have been repeated as follows: 2 repeats (Figs 3g,h,j,k, 5a,b and 7c,d), 3 repeats (Figs 1f,g and 6g,i–l and Supplementary Fig. 7c,e–i), 5 repeats (Figs 2a–c,i, 3a,b,i, 4a–e, 5c–f, 6a–e,m and 7a,b,e–h and Supplementary Figs 2, 4, 5, 6 and 7a,b,d), 6 repeats (Fig. 3d–f and Supplementary Fig. 3).

Data availability. Patient data supporting the analyses in Fig. 1 and Supplementary Fig. 1 are accessed from the public breast cancer data sets EMBL-EBI (accession numbers E-MTAB-365 and E-TABM-43) as well as GEO (accession numbers GSE16446, GSE22093, GSE3494). Statistical source data supporting Figs 3j,h,j,k; 5a,b; 6j; and 7c; and Supplementary Figs 5h; and 7b,i are provided in Supplementary Table 1. All other data supporting the findings of this study are available from the corresponding authors on request.



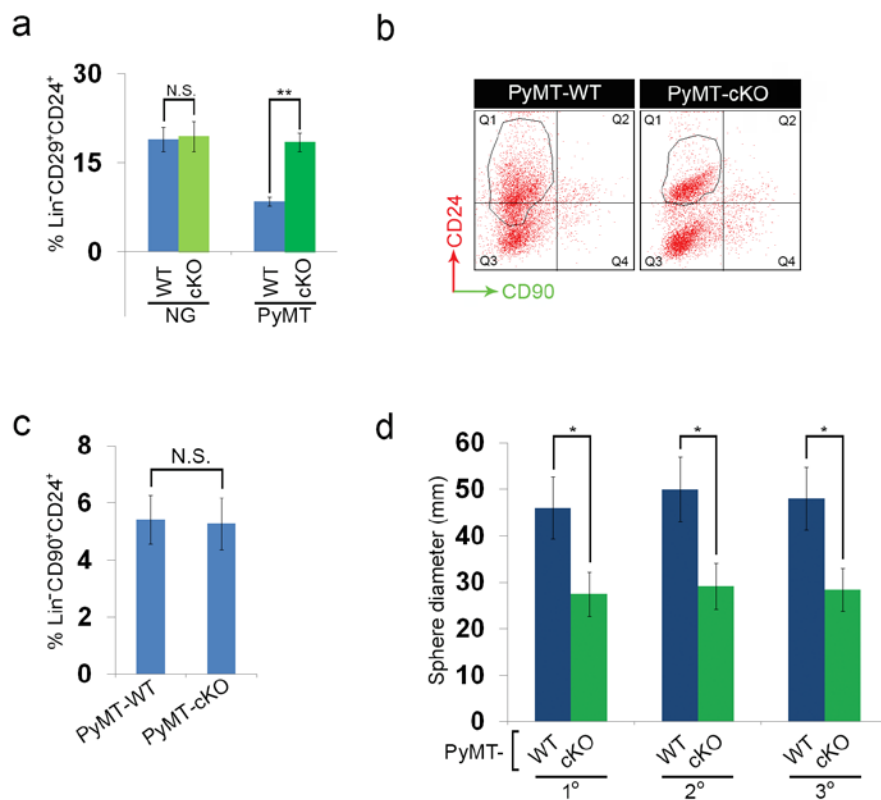
Supplementary Figure 1 A relationship between relapse-free survival rate and *Snail1* expression level in different molecular subtypes of breast cancer patients. **(a,b)** Kaplan-Meier survival analysis of the relationship between relapse-free survival (RFS) rates and *Snail1* expression level in HER2⁺ **(a)** or basal **(b)** subtype of breast cancer

patients bearing wild-type or mutant *TP53* alleles. Survival data are fitted by the “survfit” function. Kaplan-Meier curves are drawn by the “ggsurv” function in R package “survival”. Differences between two survival curves are measured by the G-rho family of tests. n represents number of patients.



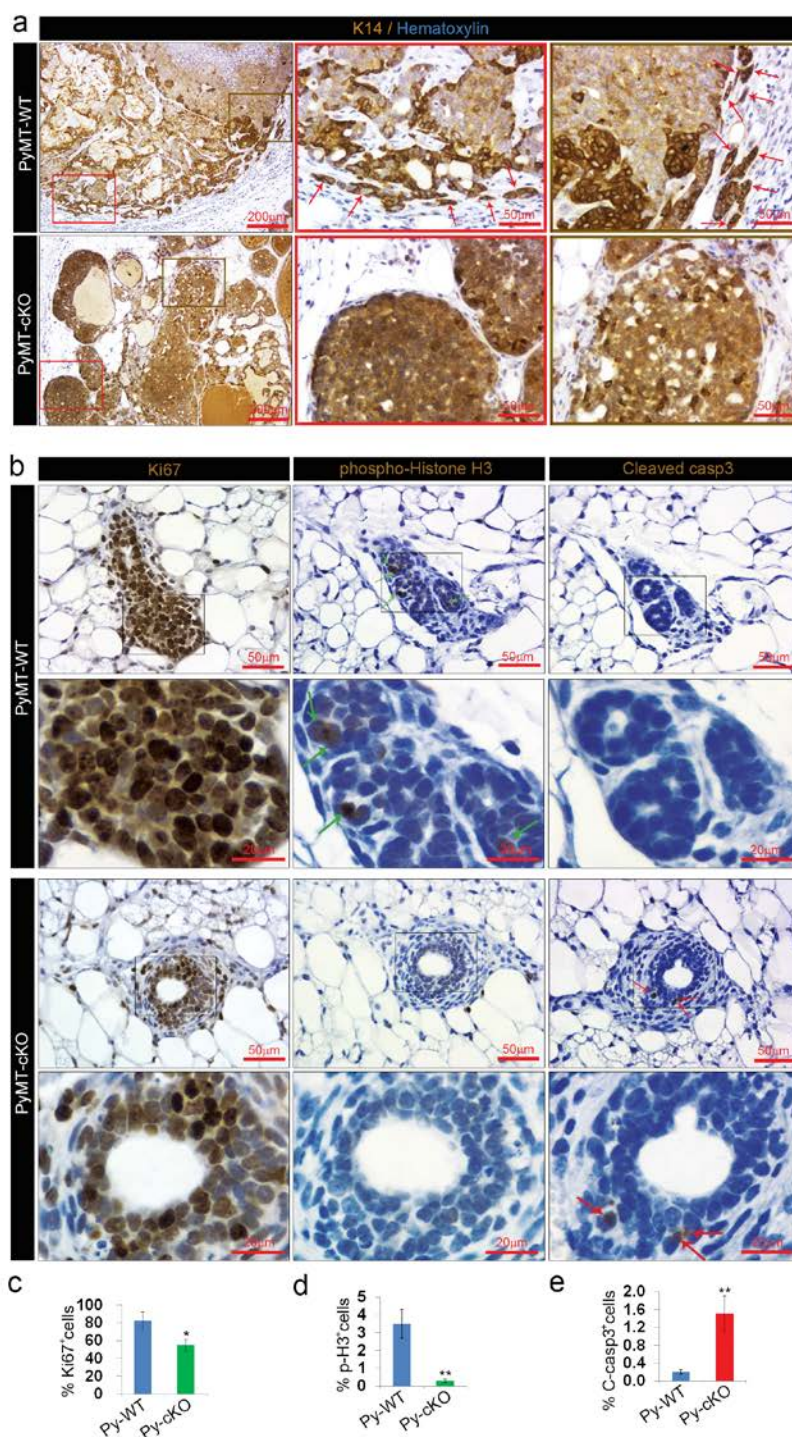
Supplementary Figure 2 *Snail1* excision in MaECs impairs PyMT-induced tumour progression without affecting mammary gland development or lactation. (a) Cross-sections of X-gal/LacZ staining in 7 wk-old preneoplastic glands (left panel) and 19 wk-old primary tumours (right panel) derived from PyMT-cKO; ROSA-LacZ mice (the image is representative of images from 5 mice). Strong X-gal/LacZ staining is detected in the epithelium, but not stromal compartment. (b) Western blot analysis of Lin^pNECs or Lin⁻NECs derived from preneoplastic glands (7 wks of age) and neoplastic tumours (19 wks of age) of PyMT-WT

and PyMT-cKO; ROSA-LacZ mice (results are representative of five independent experiments). (c) Gross view of primary tumours isolated from 15 wk-old PyMT-WT and PyMT-cKO mice (the image is representative of images from 5 mice). Dashed areas outline the primary tumours developing from the proximal to distal sites of the mammary glands. (d) Whole-mount Carmine red staining of mammary glands from WT and cKO mice at 5, 9 and 15 weeks of age as well as lactation day 3 (the image is representative of images from 5 mice). Unprocessed blots are shown in Supplementary Fig. 8.



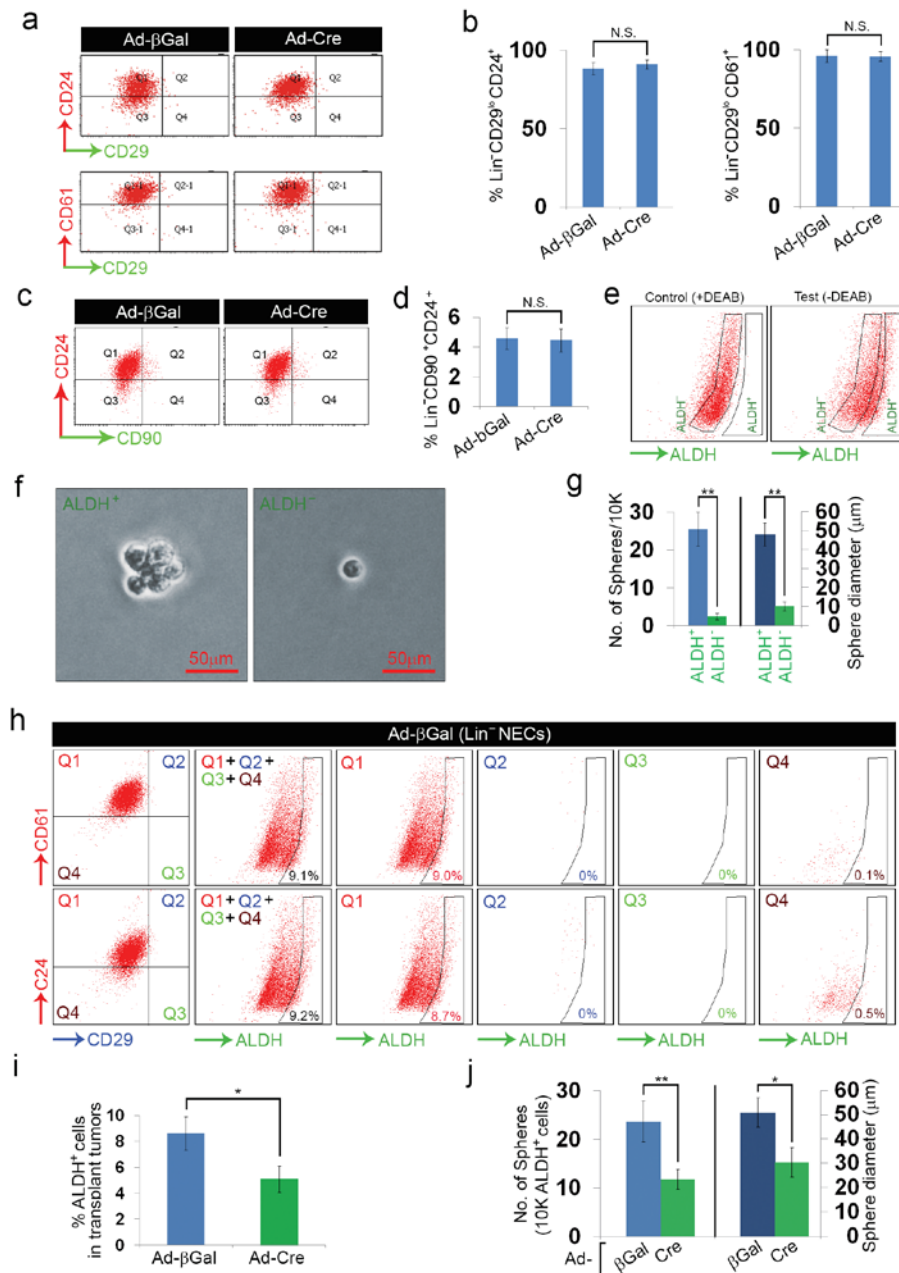
Supplementary Figure 3 Flow cytometry analysis of preneoplastic glands from PyMT-WT and -cKO mice. **(a)** Quantification of Lin⁻CD29⁺CD24⁺ basal subpopulation in normal glands from WT and cKO mice as well as preneoplastic glands from PyMT-WT and -cKO mice. Data are presented as mean ± SEM (n=6 independent experiments). **p<0.01, two-sided Student's t test. **(b)** Flow cytometry of Lin⁻CD29⁺CD90⁺ subpopulation in preneoplastic glands from PyMT-WT and -cKO mice (the image is representative of images from 6 mice)..

(c) Quantification of Lin⁻CD29⁺CD90⁺ subpopulation in preneoplastic glands as described in **(b)**. Data are presented as mean ± SEM (n=6 independent experiments). N.S., not significant, two-sided Student's t test. **(d)** Size of tumourspheres formed by PyMT-WT or -cKO pNECs dissected from mammary glands of 6 wk-old mice. 1°, 2° and 3° denote the three successive generations of pNECs used in the assay, respectively. Data are presented as mean ± SEM (n=6 independent experiments). **p<0.01, two-sided Student's t test.



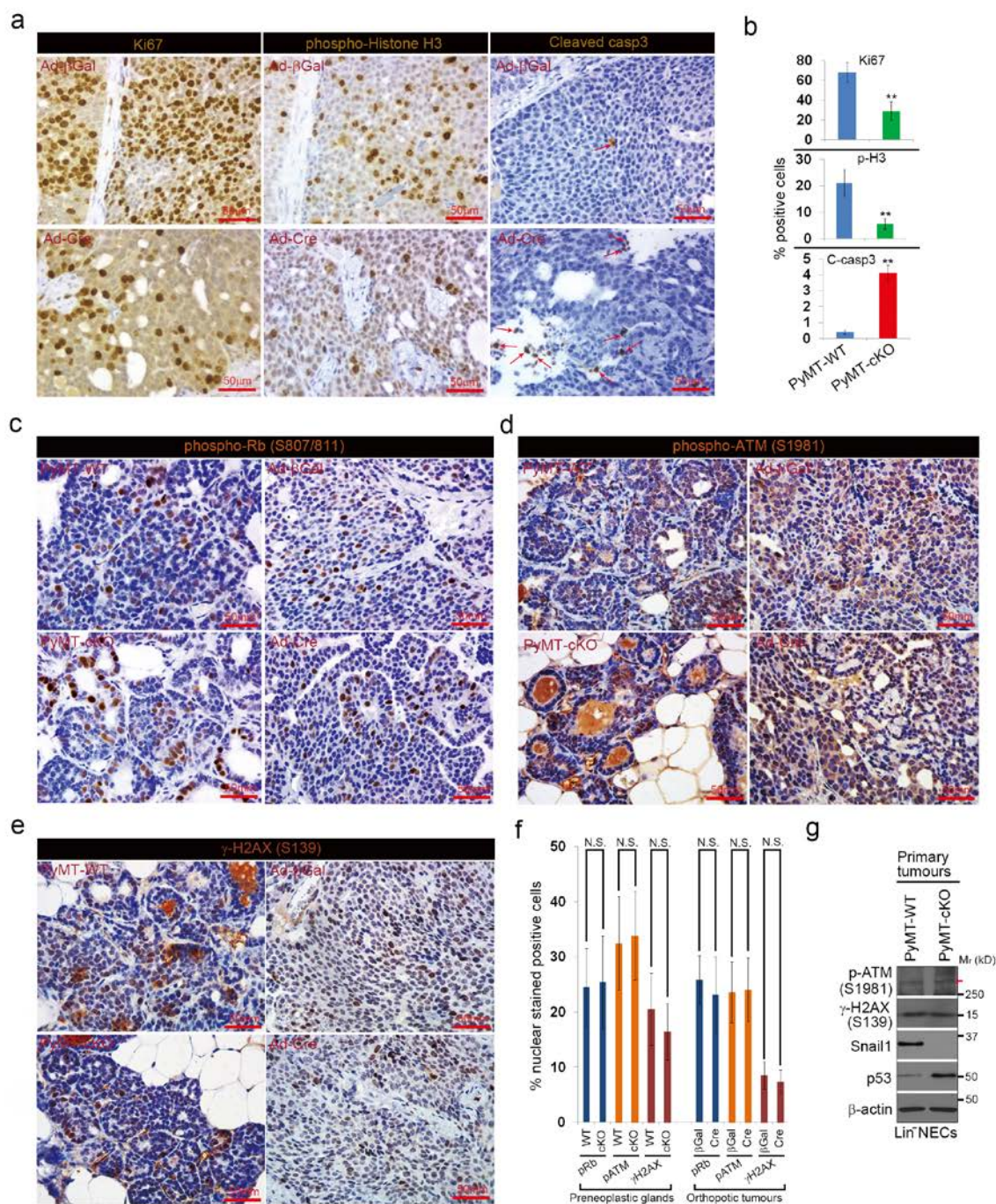
Supplementary Figure 4 Preneoplastic glands and advanced tumours from PyMT-cKO mice exhibit defects in collective invasion, proliferation and survival. **(a)** Immunohistochemical staining of K14 expression at the tumour-stromal borders in primary tumours isolated from 13 wk-old PyMT-WT and -cKO mice (the image is representative of images from 5 mice). Magnified images of boxed areas in red and brown (at left) are shown in the middle and right panels, respectively. Arrows mark invasive strands that are characteristic of K14⁺ invading leader cells at the tumour-stromal borders. **(b)** Immunohistochemical staining of Ki67, phospho-Histone H3 and cleaved caspase 3 in the preneoplastic mammary glands

of 4 wk-old PyMT-WT and -cKO females (the image is representative of images from 5 mice). Magnified areas of boxed sections are shown in the bottom panels. Green arrows in middle panels denote phospho-Histone H3-positive cells (i.e., proliferative cells). Red arrows in right panels denote cleaved caspase 3-positive cells (i.e., apoptotic cells). **(c-e)** Quantification of Ki67 **(c)**, phospho-Histone H3 (p-H3; **d**) and cleaved caspase 3 (C-casp3; **e**) positive cells (%) as shown in **(b)**. One thousand to two thousand cells were counted in 10 random fields of each slide. Data are presented as mean \pm SEM (n=5 independent experiments). *p<0.05, **p<0.01, two-sided Student's t test.



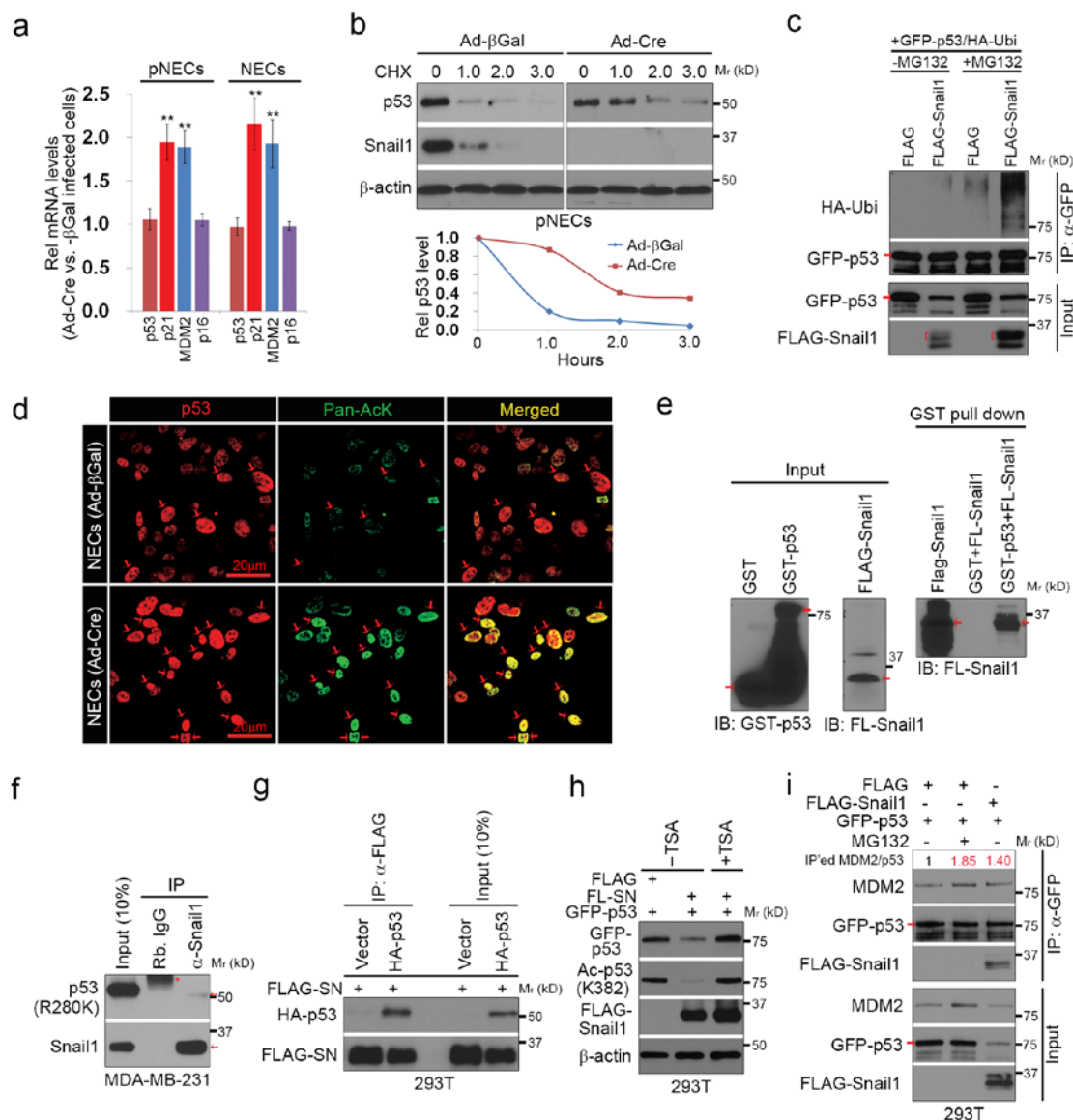
Supplementary Figure 5 Snail1 maintains TIC function in established adenocarcinomas. **(a)** Flow cytometry analysis (CD24/CD29/CD61 profiling) of LIN⁻ mammary epithelial cells isolated from transplanted tumours (n=5, each) that were derived from adeno-βGal or -Cre transduced *Snail1^{fl/fl}* adenocarcinoma cells. Tumours were retrieved 9 wks post-transduction. **(b)** Quantification of LIN⁻CD29^{lo}CD24⁺/LIN⁻CD29^{lo}CD61⁺ subpopulations in control and Snail1-deleted orthotopic tumours. Data are presented as mean ± SEM (n=5 independent experiments). NS, not significant, two-sided Student's t test. **(c)** Flow cytometry analysis (CD24/CD90 profiling) of LIN⁻ mammary epithelial cells isolated from transplanted tumours (the image is representative of images from 5 mice) as described in **(a)**. **(d)** Quantification of LIN⁻CD24⁺CD90⁺ subpopulations in control and Snail1-deleted orthotopic tumours. Data are presented as mean ± SEM (n=5 independent experiments). NS, not significant, two-sided Student's t test. **(e)** Flow cytometry analysis of ALDH activity of LIN⁻ mammary epithelial cells isolated from transplanted tumours (the image is representative of images from 5 tumours) that were derived from *Snail1^{fl/fl}* adenocarcinoma

cells. Tumours were retrieved 9 wks post-transduction. DEAB-treated samples were used as gating control (left panel). **(f,g)** Sorted Lin⁻ALDH⁻ and Lin⁻ALDH⁺ cells from transplanted tumours as described in **(e)** were subjected to tumoursphere formation assay. Representative tumourspheres are shown **(f)** with quantification of tumoursphere formation (number and size) **(g)**. Data are presented as mean ± SEM (n=5 independent experiments). **p<0.01, two-sided Student's t test. **(h)** Flow cytometry analysis (CD24/CD61/CD29/ALDH profiling) of Lin⁻ mammary epithelial cells isolated from 5 tumours) as described in **(e)**. **(i)** Quantification of Lin⁻ALDH⁺ TICs isolated from control and Snail1-deleted orthotopic tumours. Data are presented as mean ± SEM (n=5 independent experiments). *p<0.05, two-sided Student's t test. **(j)** Quantification of tumoursphere formation (number and size) by adeno-βGal or -Cre transduced Lin⁻ALDH⁺ cells sorted from transplanted tumours as described in **(e)**. Data are presented as mean ± SEM (n=5 independent experiments). *p<0.05, **p<0.01, two-sided Student's t test. Source data are provided in Supplementary Table 1 **(h)**.



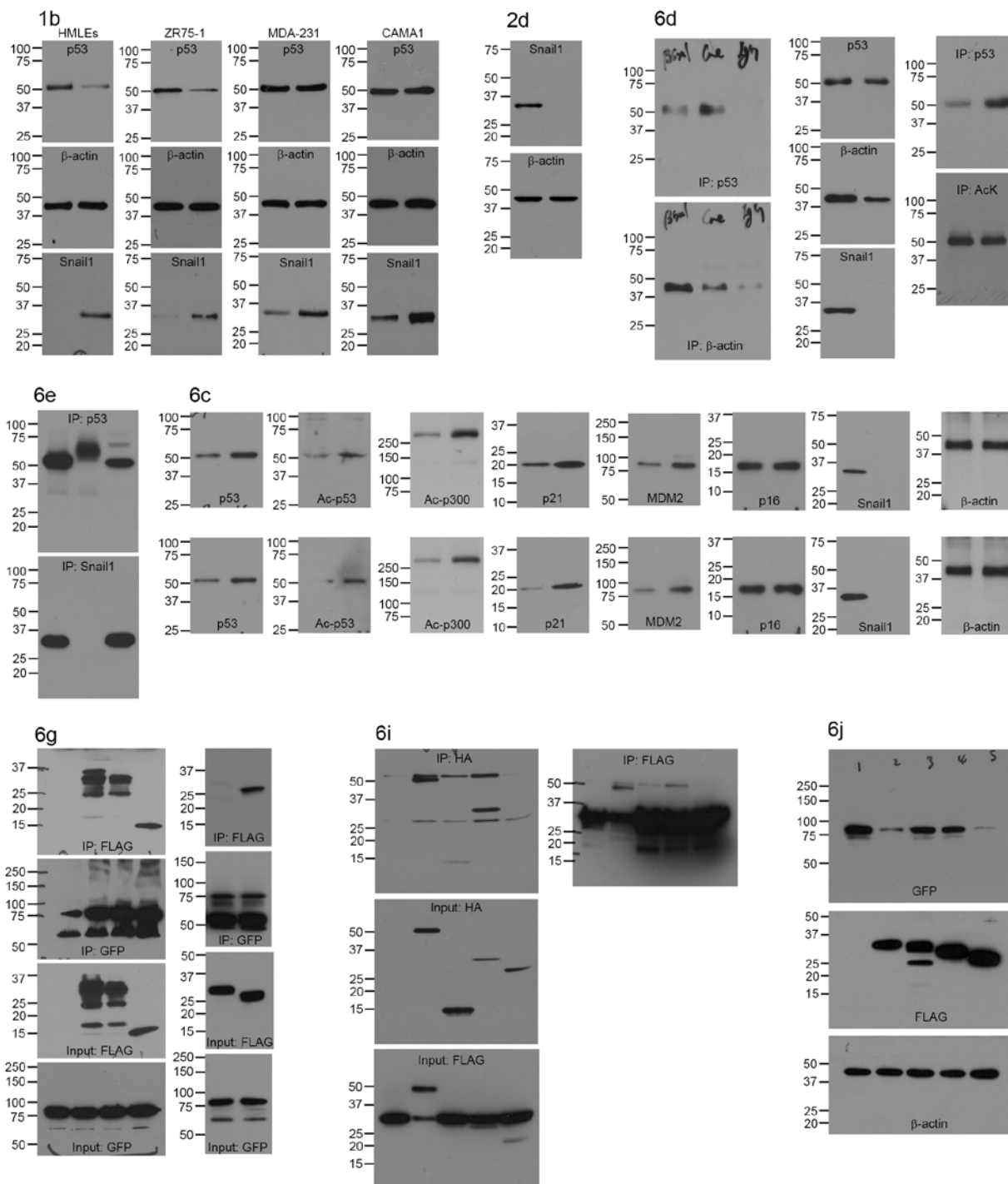
Supplementary Figure 6 Deletion of Snail1 represses tumour proliferation and survival but does not affect Rb activity or induce DNA damage in PyMT-induced tumours. **(a)** Immunohistochemical staining of Ki67, phospho-Histone H3 and cleaved caspase 3 in control and Snail1-deleted orthotopic tumours (the image is representative of images from 5 tumours). Red arrows in panels to the right indicate cleaved caspase 3-positive cells. **(b)** Quantification of Ki67, phospho-Histone H3 (p-H3) and cleaved caspase 3 (C-casp3) positive cells (%) as shown in **(a)**. One thousand to two thousand cells were counted in 10 random fields of each slide. Data are presented as mean \pm SEM (n=5 independent experiments). **p<0.01, two-sided Student's t test. **(c-e)** Immunohistochemical staining of p-Rb **(c)**, p-ATM **(d)** and γ -H2AX **(e)** in preneoplastic glands of 7 wk-old PyMT-WT or

PyMT-cKO mice (left panels) or formed from neoplastic Snail1^{fl/fl} mammary epithelial cells that were transduced with adeno- β Gal or -Cre prior to a 9 wk transplantation period (right panels). The image is representative of images from 5 mice or orthotopic tumours. **(f)** Quantification of p-Rb, p-ATM and γ -H2AX positive cells (%) as shown in **(c-e)**. One thousand to two thousand cells were counted in 10 random fields of each slide. Data are presented as mean \pm SEM (n=5 independent experiments). NS, not significant, two-sided Student's t test. **(g)** Immunoblot analysis of Lin⁺NECs isolated from primary tumours of 12 wk-old PyMT-WT and PyMT-cKO mice (the image is representative of images from 5 mice). Arrows denote the specific bands with their expected molecular weights. Unprocessed blots are shown in Supplementary Fig. 8.

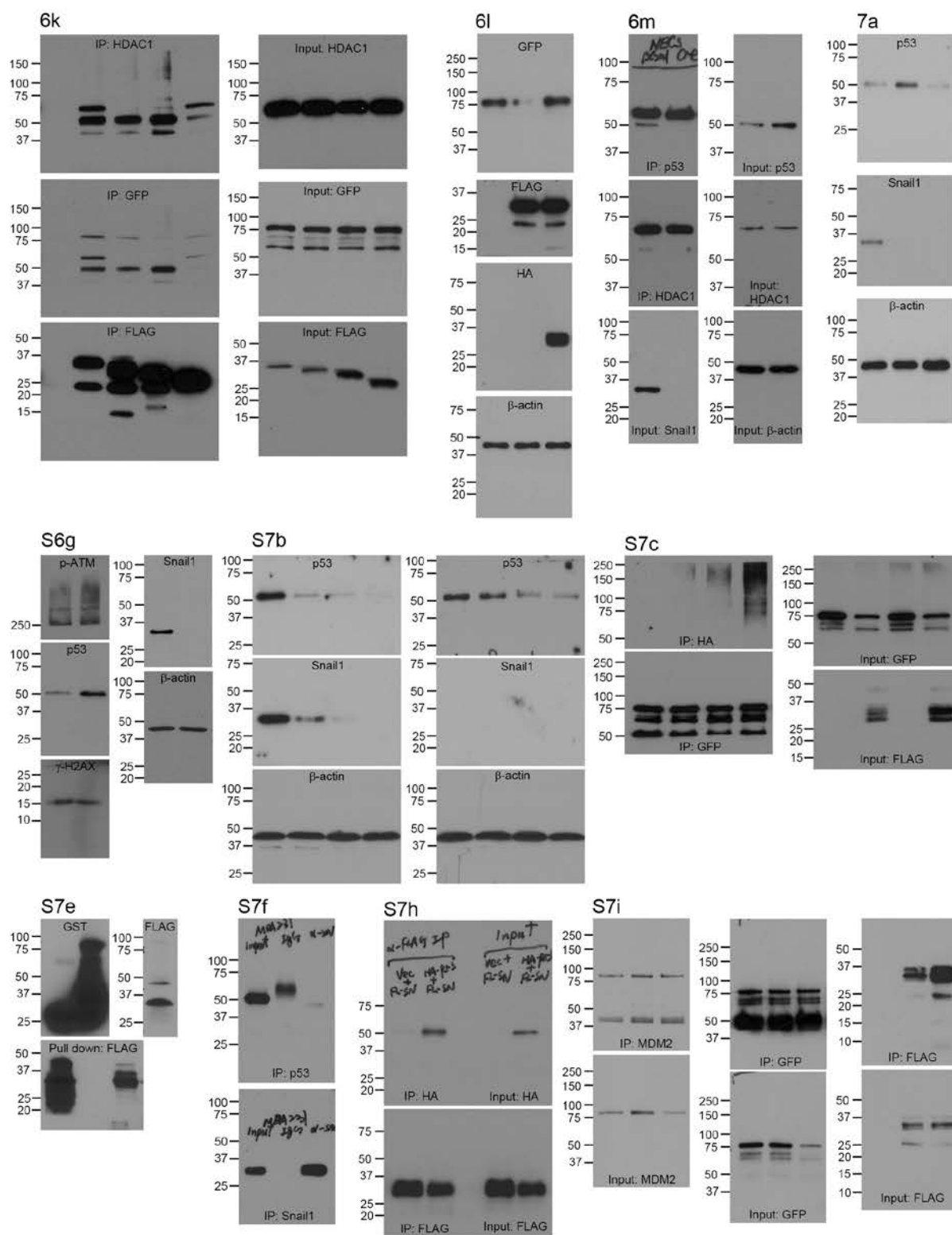


Supplementary Figure 7 Snail1 binds and negatively regulates p53 protein levels. **(a)** pNECs or NECs were recovered from 7 wk-old or 19 wk-old PyMT-WT mice, respectively. Cells were transduced with adeno-βGal or -Cre, and subjected to RT-PCR analysis. Data are presented as mean ± SEM (n=5 independent experiments). **p<0.01, one-way ANOVA test. **(b)** Cycloheximide (CHX; 100 μg/ml) pulse-chase analysis of p53 protein levels in control or Snail1-deleted pNECs as shown in **(a)**. Quantification of p53 protein expression levels are shown in bottom panel. **(c)** 293T cells were co-transfected with the indicated plasmids at a ratio of 1:10 and treated with MG132 (10 μM) for 6 h. Cell lysates collected for IP analysis. **(d)** Immunofluorescent staining of p53 and Pan-AcK in NECs as described in **(c)**. Arrows denote the cells expressing comparable levels of p53 between adeno-βGal and -Cre transduced cells. **(e)** GST control or GST-p53 protein bound to GST beads was co-incubated with FLAG-tagged Snail1 protein purified from rabbit reticulocyte lysates, and the

mixture subjected to GST pull-down assays. **(f)** Lysates from MDA-MB-231 cells were subjected to IP assay. **(g)** 293T cells were co-transfected with equal amount of HA-p53-WT and FLAG-Snail1, and the cell lysates were prepared and subjected to IP analysis. **(h)** 293T cells co-transfected with GFP-p53 and FLAG-Snail1 at a ratio of 1:10, and then treated with 1 μM trichostatin A (TSA) for 24 h. Cell lysates were prepared for immunoblotting. **(i)** 293T cells were co-transfected with the indicated plasmids at a ratio of 1:1:10 and treated with DMSO or MG132 (10 μM) for 6 h. Cell lysates collected for IP analysis. The numbers shown in the blots are the ratios of MDM2/p53 in the IP'ed products. Blots are representatives of three independent experiments. Asterisks and arrows denote IgGs and specific bands with their expected molecular weights, respectively. Results are representatives of three **(c,e-i)** or five **(b,d)** independent experiments. Unprocessed blots are shown in Supplementary Fig. 8. Source data are provided in Supplementary Table 1 **(b,i)**.



Supplementary Figure 8 Unprocessed images of blots. Uncropped images of scanned western blots shown in Figures and Supplementary Figures are provided.



Supplementary Figure 8 continued

Supplementary Table 1 Statistical source data. All data are organized into different sheets tagged by the corresponding figure numbers.

Sheet 1 corresponding to Fig. 3g,h,j,k

Sheet 2 corresponding to Fig. 5a,b

Sheet 3 corresponding to Fig. 6j

Sheet 4 corresponding to Fig. 7c

Sheet 5 corresponding to Supplementary Fig. 5h

Sheet 6 corresponding to Supplementary Fig. 7b,i